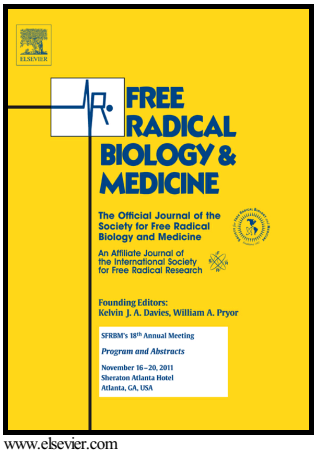

Manganese porphyrin redox state in endothelial cells: resonance Raman studies and implications for antioxidant protection towards peroxynitrite

Sebastián Carballal, Valeria Valez, Damián Alvarez-Paggi, Artak Tovmasyan, Ines Batinic-Haberle, Gerardo Ferrer-Suetac, Daniel H. Murgida, Rafael Radi

PII: S0891-5849(18)31438-2
DOI: https://doi.org/10.1016/j.freeradbiomed.2018.08.023
Reference: FRB13887

To appear in: *Free Radical Biology and Medicine*

Received date: 15 April 2018
Revised date: 18 August 2018
Accepted date: 20 August 2018

Cite this article as: Sebastián Carballal, Valeria Valez, Damián Alvarez-Paggi, Artak Tovmasyan, Ines Batinic-Haberle, Gerardo Ferrer-Suetac, Daniel H. Murgida and Rafael Radi, Manganese porphyrin redox state in endothelial cells: resonance Raman studies and implications for antioxidant protection towards peroxynitrite, *Free Radical Biology and Medicine,* https://doi.org/10.1016/j.freeradbiomed.2018.08.023

Manganese porphyrin redox state in endothelial cells: resonance Raman studies and implications for antioxidant protection towards peroxynitrite

Sebastián Carballal [a,b1], Valeria Valez [a,b1], Damián Alvarez-Paggi[d2], Artak Tovmasyan [e], Ines Batinic-Haberle[e], Gerardo Ferrer-Suetac[,b], Daniel H. Murgida[d], Rafael Radi [a,b,*]

[a]Departamento de Bioquímica, Universidad de la República, Montevideo, Uruguay

[b]Center for Free Radical and Biomedical Research, Facultad de Medicina, Universidad de la República, Montevideo, Uruguay

[c]Laboratorio de Fisicoquímica Biológica, Facultad de Ciencias, Universidad de la República, Montevideo, Uruguay;

[d]Departamento de Química Inorgánica, Analítica y Química Física and INQUIMAE-CONICET, Facultad de Ciencias Exactas y Naturales, Universidad de Buenos Aires, Ciudad Universitaria, Pab. 2, piso 1, C1428EHA-Buenos Aires, Argentina;

[e]Department of Radiation Oncology, Duke University Medical Center, Durham, NC 27710, USA.

*****Correspondence should be addressed to Rafael Radi, Departamento de Bioquímica, Facultad de Medicina, Avda. Gral. Flores 2125; 11800 Montevideo, Uruguay; Phone: +598-29249561; Fax: +598-29249563; E-mail: rradi@fmed.edu.uy.

[1] These authors contributed equally.

[2] Present Address: Instituto de Investigaciones Bioquímicas de Buenos Aires, FIL-CONICET

ABSTRACT

Manganese(III) cationic *ortho N*-substituted pyridylporphyrins (MnP) act as efficient antioxidants catalyzing superoxide dismutation and accelerating peroxynitrite reduction. Importantly, MnP can reach mitochondria thereby offer protection against reactive species in different animal models of disease. Although an LC-MS/MS-based method for MnP quantitation and subcellular distribution has been reported, a *direct* method capable of evaluating both the uptake and the redox state of MnP in living cells has not yet been developed. In the present work we applied resonance Raman (RR) spectroscopy to analyze the intracellular accumulation of two potent MnP-based lipophilic SOD mimics, MnTnBuOE-2-PyP^{5+} and MnTnHex-2-PyP^{5+} within endothelial cells. RR experiments with isolated mitochondria revealed that the reduction of Mn(III)P was affected by inhibitors of the electron transport chain, supporting the action of MnP as efficient redox active compounds in mitochondria. Indeed, RR spectra confirmed that MnP added in the Mn(III) state can be incorporated into the cells, readily reduced by intracellular components to the Mn(II) state and oxidized by peroxynitrite. To assess the combined impact of reactivity and bioavailability, we studied the kinetics of Mn(III)TnBuOE-2-PyP^{5+} with peroxynitrite and evaluated the cytoprotective capacity of MnP by exposing the endothelial cells to nitro-oxidative stress induced by peroxynitrite. We observed a preservation of normal mitochondrial function, attenuation of cell damage and prevention of apoptotic cell death. These data introduce a novel application of RR spectroscopy for the direct detection of MnP and their redox states inside living cells, and helps to rationalize their antioxidant capacity in biological systems.

Graphical abstract

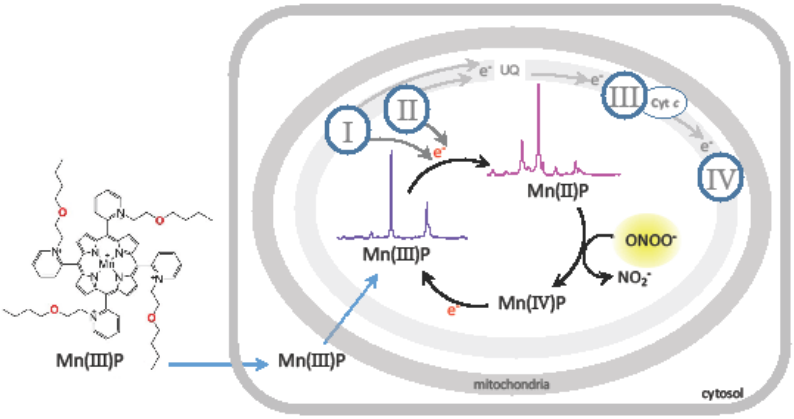

ABBREVIATIONS

[1]The abbreviations used are: Manganese porphyrins (MnPorphyrins or MnP); Mn(III)TnHex-2-PyP^{5+}, manganese(III) *meso*-tetrakis((*N*-*n*-hexyl)pyridinium-2-yl)porphyrin; Mn(III)TnBuOE-2-PyP^{5+}, manganese(III) *meso*-tetrakis(*N*-*n*-butoxyethylpyridinium-2-yl)porphyrin (BMX-001); BAEC, bovine aortic endothelial cells; RR, Resonance Raman; SIN-1, 1,3-morpholinosydnonimine; Fl-B, Fluorescein-based boronate; NOC-7, 3-(2-Hydroxy-1-methyl-2-nitrosohydrazino)-N-methyl-1-propanamine; FCCP, carbonyl cyanide 4-(trifluoromethoxy)phenylhydrazone; AA, antimycin A; R, rotenone.

Keywords: Manganese porphyrin; Peroxynitrite; Endothelial cells; Mitochondria; Resonance Raman

INTRODUCTION

Several metalloporphyrins have been identified as potent catalysts of numerous redox reactions; in particular, manganese porphyrins (MnP) were found very early to act as efficient catalytic antioxidants (1,2). For instance, they can act as superoxide dismutase (SOD) mimics catalyzing the dismutation of superoxide ($O_2^{\bullet-}$) (3-6). They can react fast with carbonate radical ($CO_3^{\bullet-}$) (8) and also catalyze the dismutation of H_2O_2 with much lower rate constant (7). Among synthetic scavengers, MnP are the fastest reductants of peroxynitrite[3] (9-12), a powerful oxidizing and nitrating agent, that can be formed *in vivo* by the diffusion-controlled reaction between the free radicals nitric oxide ($^{\bullet}NO$) and $O_2^{\bullet-}$. Those cationic MnP that are potent SOD mimics have electron-deficient Mn site. The presence of charges close to the Mn site in the *ortho* positions of the pyridyl rings makes them electron-deficient and affords both thermodynamic and kinetic facilitation for the reactions with electron-rich anionic reactive species, such as $O_2^{\bullet-}$, $CO_3^{\bullet-}$ and also peroxynitrite (3,4,13).

Mn(III)P can reduce peroxynitrite by one or two-electron mechanisms. One-electron reduction leads to the formation of nitrogen dioxide radical ($^{\bullet}NO_2$) and O=Mn(IV)Porphyrin, with rate constants in the ~ 10^5 - 10^7 M^{-1} s^{-1} range at pH 7.4 and 37 ºC (8,14). The oxidized manganese complex O=Mn(IV)P can be fast reversed to Mn(III)P by the available endogenous reductants *e.g.* ascorbate, urate or glutathione, completing a catalytic cycle of peroxynitrite reduction (eq. 1-2) (9-12,15). Although this

[3] The term peroxynitrite is used to refer to the sum of peroxynitrite anion ($ONOO^-$) and peroxynitrous acid (ONOOH, pK_a ~ 6.8). IUPAC recommended names are oxoperoxonitrate(1−) and hydrogen oxoperoxonitrate, respectively.

cycle is very efficient, it does not inactivate the oxidizing power of peroxynitrite but deviates it towards the formation of two oxidants, O=Mn(IV)P and $^{\bullet}NO_2$ which can mediate pro-oxidant actions, for instance tyrosine nitration.

$$Mn(III)P^{5+} + ONOO^{-} \rightarrow O{=}Mn(IV)P^{4+} + {}^{\bullet}NO_2 \quad (1)$$

$$O{=}Mn(IV)P^{4+} + RedH + H^{+} \rightarrow Mn(III)P^{5+} + {}^{\bullet}Red + H_2O \quad (2)$$

Moreover, Mn(III)P can be reduced by several biological reductants (RedH) such as glutathione, ascorbate, tetrahydrobiopterin, or enzymatically by oxidoreductases, and most notably flavoenzymes such as succinate dehydrogenase and NADH dehydrogenase of the mitochondrial electron transport chain (16-18). The resulting Mn(II)P can promote the two-electron reduction of peroxynitrite to nitrite (NO_2^{-}) instead of $^{\bullet}NO_2$ (eq. 3), protecting sensitive targets from peroxynitrite or its radical derived-mediated damage.

$$Mn(II)P^{4+} + ONOO^{-} \rightarrow O{=}Mn(IV)P^{4+} + NO_2^{-} \quad (3)$$

Under basal physiological conditions, mitochondria represents a major source of oxidants, rendering it one of the key subcellular compartments where peroxynitrite is generated (19,20). Intramitochondrial peroxynitrite formation is inhibited by superoxide dismutase (MnSOD) and, once formed, decomposed by peroxidatic enzymes such as peroxiredoxins 3 and 5, which constitute the key defensive lines in protecting the cell from oxidative damage (21-23). However, if an increase in the mitochondrial generation of reactive species surpasses the antioxidant protection, relevant consequences include peroxynitrite-triggered nitro-oxidative modifications. These modifications on target

biomolecules such as oxidation and inactivation of proteins and lipid components, depending on the extent of the chemical modifications, can cause alterations of mitochondrial homeostasis, potentially leading to cell death (20,24-26). Therefore, modulation of oxidants formation can limit the initiation and progression of different diseases related to mitochondrial dysfunction (27-31). In this sense, overexpression of antioxidant enzymes and the development of mitochondrially-targeted antioxidants have been reported to play protective effects against the toxicity of reactive species (27-32). Among synthetic scavengers, MnP were found to exert strong protective effects against peroxynitrite-mediated cytotoxicity, and have been successfully used in different pathophysiological conditions, for example in models of vascular and neuronal degeneration involving peroxynitrite formation (33,34). Also, in a model of LPS-induced sepsis in rats, MnP were able to ameliorate mitochondrial and diaphragmatic dysfunction, preventing organ failure during severe sepsis (35). It is important to note that in addition to the fast reaction with peroxynitrite, $O_2^{\bullet-}$ and $CO_3^{\bullet-}$, the antioxidant efficiency of MnP observed *in vivo* depends on their bioavailability, i.e. tissue, cellular, and subcellular distribution, which in turn depends on the nature of *N*-pyridyl substituents that may modify the bulkiness (size and shape), charge and lipophilicity (36-38). With the aim to enhance the biodistribution of MnP, the original structure of the Mn(III)meso-tetrakis(*N*-ethylpyridinium-2-yl)porphyrin) (MnTE-2-PyP^{5+}) was adjusted lengthening the alkyl chains on the porphyrin substituents, resulting in a new generation of lipophilic analogs. Among them, the Mn(III)meso-tetrakis((*N*-n-hexyl)pyridinium-2-yl)porphyrin (Mn(III)TnHex-2-PyP^{5+}) has been frequently MnP studied (38-42). More recently, the synthesis of new MnP with the insertion of oxygen atoms within the alkyl chains, resulted in Mn(III)meso-tetrakis(N-n-butoxyethylpyridinium-2-yl)porphyrin (Mn(III)TnBuOE-2-PyP^{5+}), which showed less

toxicity while maintaining high lipophilicity (43). Importantly, MnTnBuOE-2-PyP^{5+} is currently in Phase I/II clinical trials as a radioprotector of normal tissues in cancer patients (glioma, head and neck and anal cancer patients) (44,45). The remarkable efficacy of MnP protection on a variety of oxidative stress-related disease models may be at least in part attributed to their ability to cross cell membranes and accumulate in mitochondria, mimicking location and function of the mitochondrial enzyme, MnSOD (46-48). Also, MnP colocalization with mitochondrial redox partners would activate their function as catalytic antioxidants in the same location where oxidants, and particularly peroxynitrite, can be formed (33,38,42,49-56).

Efforts have been made in order to develop methodologies to assess tissue and subcellular distributions of MnP. One of the analytical methods reported involves subcellular fractionation, substitution of the porphyrin Mn(II) site with Zn(II), followed by fluorimetric detection and LC-MS/MS quantification (57-59). Previous studies on cell incorporation, have observed the effect of MnP on SOD-deficient bacteria and yeast, which grow very poorly in the presence of oxygen. Since some MnP possess high SOD activity, they are able to rescue and support the aerobic growth and thus, their beneficial effect can be associated with its facile incorporation and high reactivity (60-64). Although these assays provide valuable information, a *direct* method to evaluate the uptake and redox state of MnP in living cells has not been yet developed. With this need in mind, here we explore the potential of Raman spectroscopy as an alternative method. In this technique the vibrational spectrum of a sample is obtained from the inelastic scattering of an incident laser beam. In sharp contrast to vibrational spectroscopies based on infrared light absorption, water is essentially Raman inactive, thus making this method particularly suited for biological samples. Moreover, if the

excitation is in resonance with an electronic transition of a chromophoric unit in the sample, the intensity of the resulting resonance Raman (RR) spectrum solely of this chromophore is enhanced by several orders of magnitude over the background spectrum of non-resonant molecules. In this way, the choice of the laser excitation line represents a simple and effective means to achieve high sensitivity and molecular selectivity in complex samples. Interestingly, RR measurements are rapid, non-destructive, non-invasive and can be easily adapted to different sampling schemes, from simple quartz cuvettes to remote optical fiber probes or confocal microscopes, among others. RR spectroscopy has long been employed for the detection and characterization of heme proteins (65-68) and free porphyrins (69-72) due to the very high RR cross-section of porphyrins, particularly when excited in resonance with the Soret absorption band, and because the spectra allow to discriminate the redox state, spin and coordination of the central metal ion.

In the present study, we have employed RR spectroscopy in order to detect the intracellular accumulation of MnTnBuOE-2-PyP^{5+} and MnTnHex-2-PyP^{5+} within bovine aortic endothelial cells (BAEC) and also monitored in real time their reduction by intracellular components, in particular those of the mitochondrial electron transport chain. In addition, RR allowed distinguishing the redox state changes of MnP in endothelial cells or isolated mitochondria exposed to peroxynitrite. We have also characterized the reaction kinetics of MnTnBuOE-2-PyP^{5+} with peroxynitrite and evaluated the antioxidant cytoprotective capacity of these compounds in biological systems.

EXPERIMENTAL PROCEDURES

Reagents.

Reagents were purchased from Sigma-Aldrich (St. Louis, MO) and used as received unless otherwise indicated. The manganese porphyrins used: MnTnHex-2-PyP^{5+}, manganese(III) *meso*-tetrakis((*N*-*n*-hexyl)pyridinium-2-yl)porphyrin and MnTnBuOE-2-PyP^{5+}, manganese(III) *meso*-tetrakis(*N*-*n*-butoxyethylpyridinium-2-yl)porphyrin were synthesized as described previously (40,43,73). Culture medium 199 (M199) and fetal bovine serum (FBS) were obtained from GIBCO (Invitrogen, Grand Island NY). Fluorescein boronate-based probe (Fl-B) was synthesized as reported previously (74). Annexin-V-FITC Alexa fluor 488 was obtained from Molecular Probes-Invitrogen (Eugene, OR) and propidium iodide was from Calbiochem. Peroxynitrite was synthesized from hydrogen peroxide and sodium nitrite under acidic conditions in a quenched flow reactor as described previously (75,76). Excess hydrogen peroxide was removed by treatment with manganese dioxide. Peroxynitrite concentration was determined at 302 nm (ε = 1670 M^{-1} cm^{-1} (77)) and nitrite contamination was typically less than 25 % with respect to peroxynitrite. Stock solutions were stored at -80 °C and diluted in 0.1 M NaOH immediately before use.

Spectroscopic methods.

Resonance Raman (RR) spectra were acquired in backscattering geometry using a confocal microscope (Olympus BX41) equipped with a long working distance objective (Nikon 20x. N.A. 0.35) and coupled to a single stage spectrograph (Jobin Yvon XY-800) equipped with 1800 lines/mm grating and liquid nitrogen cooled back illuminated CCD detector. Rayleigh radiation was rejected using a razor edge filter (Semrock). Typically ca. 100 μL of sample were placed in a cylindrical quartz cell that was rotated under the laser beam at about 5 Hz to prevent laser-induced damage. Spectra were

acquired with the 457.9 nm line of an argon ion laser (Coherent Innova 70c), i.e. in resonance with the Soret band of the porphyrins, using laser powers at sample ≤ 5 mW to avoid laser-induced damage. The spectrometer was calibrated employing Hg and Na calibration lamps (Newport) as an internal spectroscopic standard to ensure reproducibility. The reported RR spectra represent an average of 4-10 individual spectra and were measured with accumulation times of 20-60 s and increments per data point of 0.35 cm^{-1}.

Kinetics of peroxynitrite reaction with MnPorphyrin.

Oxidation of Mn(III)TnBuOE-2-PyP^{5+} with peroxynitrite was carried out under pseudo-first-order conditions with peroxynitrite in excess over the MnP. In all cases, peroxynitrite (dissolved in a NaOH) was mixed with Mn(III)TnBuOE-2-PyP^{5+} dissolved in sodium phosphate buffer. The final concentration of Mn(III)TnBuOE-2-PyP^{5+} after mixing was 0.5 μM, peroxynitrite was in excess by at least 10-fold, and sodium phosphate buffer concentration was 50 mM, at different pH values from 5.23 to 7.20, containing diethylenetriaminepentaacetic acid (DTPA, 0.1 mM) to eliminate potential metal trace interference. The temperature was maintained constant at 37.0 ± 0.1 °C, and the pH of the reaction mixtures was measured at the outlet of the stopped flow. The reaction was monitored by the change in absorbance in the Soret band of Mn(III)TnBuOE-2-PyP^{5+} at 455 nm, and the apparent rate constants (k_{obs}), were determined by fitting stopped-flow data to a single exponential function with the software provided with the instrument. The second-order rate constant was determined from the slope of the plot of k_{obs} versus peroxynitrite concentrations. All kinetic runs were performed in a stopped-flow spectrophotometer (SX20, Applied Photophysics)

with a mixing time of <2 ms. Reported values are the average of at least seven separate determinations.

Cell culture.

BAEC were obtained as described previously (78,79). Briefly, bovine thoracic aortas were acquired from a local slaughterhouse (Frigorífico Carlos Schneck, Montevideo, Uruguay), and cells were obtained by scraping the luminal surface of the aorta. When colonies of BAEC were formed, they were isolated using 8-mm diameter cloning rings (Sigma). The purity of the culture was assessed by immunocytochemistry using an anti-human von Willebrand factor polyclonal antibody (Sigma) and an acetylated low-density lipoprotein fluorescently labeled (DiI-Ac-LDL). The cells were cultivated on gelatin-coated tissue plastic and propagated by subculturing in a 1:4 ratio in M199 with 5 % FBS, 100 U/ml penicillin G, and 100 μg/ml streptomycin sulfate. Cell media was routinely changed after 3 days, 1 week after subculture, and once a week thereafter for no longer than a month. Experiments were conducted using cells at 95 % confluence and between passages 5 and 8. All treatments were performed in M199 with reduced fetal bovine serum (0.4% FBS), unless otherwise indicated.

MnP incorporation on cells and mitochondria.

BAEC were preincubated with Mn(III)P (5 μM) for 2 hours and washed twice in PBS, to remove all the non-incorporated MnP.

Alternatively, for RR studies, Mn(III)P (5 μM) were added directly to mitochondria or cells in the cylindrical quartz cell. The appropriate non-toxic concentrations of MnTnBuOE-2-PyP^{5+} and MnTnHex-2-PyP^{5+} used in this work were evaluated by the MTT assay, by exposing BAEC to increase concentrations of Mn(III)P ranging from 2

to 10 μM. There was no significant decrease in cell viability over a 2 h exposure to Mn(III)P at concentrations below 10 μM. The mitochondrial electron transport inhibitors used included: rotenone, malonate and antimycin A as inhibitors of Complex I, II and III, respectively. Alternatively to malonate, in experiments with BAEC we used thenoyl trifluoroacetate (TTFA) which also blocks the electron transfer from Complex II and can reach mitochondria without the need to add any permeabilization agent. The appropriate concentrations of the inhibitors used in our experimental conditions were tested previously.

SIN-1 exposure:

SIN-1 (1,3-morpholinosydnonimine) stock solution was prepared in 3 mM HCl and the pH was adjusted to 7.4 during assays in cell media. SIN-1 has been used in vitro to simultaneously generate $O_2^{\bullet-}$ and $^{\bullet}NO$ which react to form peroxynitrite (80), and can easily penetrate in BAEC generating an extra and intracellular peroxynitrite flux (81). The yield of peroxynitrite flux produced by the SIN-1 concentrations selected for experiments, 100 and 250 μM, produces a peroxynitrite flux of 3.14 and 7.6 μM/min, respectively, determined by oxidation of fluorescein boronate, as reported previously (74,82).

Detection of endogenous peroxynitrite in BAEC measuring FI-B oxidation.

The generation of endogenously peroxynitrite in BAEC was determined using the fluorescein-boronate probe (Fl-B), and monitored under different conditions by the increase in fluorescence intensity emission corresponding to Fl-B oxidation ($\lambda_{ex/em}$ = 492/515 nm) (74). BAEC were pre-incubated with Mn(III)TnBuOE-2-PyP^{5+} (5 μM) for 2 h and after treatment, cells were washed twice with PBS and incubated with FI-B (50

μM) for 30 min at 37 ºC. Intramitochondrial-peroxynitrite was generated by a simultaneous stimulation of $O_2^{\bullet-}$ formation with the complex III- electron transport chain inhibitor, antimycin A (4 μM) and the $^{\bullet}NO$ donor (NOC-7, 100 μM yielding ~ 8.6 μM/min $^{\bullet}NO$, at pH 7.4 and 37 ºC). The time course of FI-B in BAEC was monitored in a fluorescence plate reader at 25 ºC (Varioskan, Thermo) at λ_{ex}= 492 nm and λ_{em}= 515 nm for 20 min. Control assays showed that Mn(III)TnBuOE-2-PyP^{5+} (10 μM) added to Fl-B (50 μM) plus peroxynitrite (100 μM in bolus addition) in PBS, interfered less than 8 % with the fluorescence intensity emission corresponding to Fl-B oxidation (data not shown).

Mitochondria purification.

Rat heart mitochondria were isolated and purified by differential centrifugation as described previously (83). Briefly, rats were anesthetized, and the heart was removed and washed extensively, minced, and homogenized with a small tissue grinder. Tissue fragments were disrupted using a Potter-Elvehjem homogenizer in a solution containing: sucrose (0.3 M), MOPS (5 mM), potassium phosphate (5 mM), EGTA (1 mM), and 0.1 % bovine serum albumin (BSA) (homogenization buffer, pH 7.4). The homogenate was then centrifuged at 1500 g, and mitochondria were isolated from the supernatant by centrifugation at 13000 g. Mitochondrial pellets were resuspended in minimal volume of homogenization buffer.

Measurement of mitochondrial function in BAEC.

Mitochondrial function in BAEC was measured using a Seahorse XF24 extracellular flux analyzer (Agilent Technologies), which allows the determination of oxygen consumption rates (QO_2) and proton concentration in real time (84-86). BAEC were

plated in 24- well Seahorse microplate at an optimum seeding density (40,000 cells, (84)) and once the cells reached confluence 24 h later, Mn(III)TnBuOE-2-PyP^{5+} (5 μM) was added to allow incorporation for 2 h. Cells were washed twice with phosphate-buffered saline (PBS, 0.14 M NaCl, 0.003 M KCl, 0.002 M KH_2PO_4, 0.01 Na_2HPO_4), pH 7.4, in order to remove excess of MnP. Then cells were exposed to SIN-1 (100 μM) overnight, washed and incubated with an un-buffered Seahorse media to allow equilibration for 1 hour before the assay. Drugs were added as indicated in the experiment: Oligomycin (1 μM), FCCP (1 μM), antimycin A (AA, 1 μM) and Rotenone (R, 0.1 μM). Basic procedure for the XF24 extracellular flux analyzer was followed as described in www.agilent.com. Data are expressed as the oxygen consumption rate (QO_2) in pmol/min. From the QO_2 obtained before and after addition of drugs to the cells and corrected per μg protein, we calculated parameters related to mitochondrial function and metabolism. Non-mitochondrial QO_2 was measured adding AA/R at the end of each respiratory experiment in order to fully inhibit the mitochondrial electron transport chain. Considering that this rate is constant, it was subtracted from all other rates. Different experimental conditions yielded similar non-mitochondrial QO_2 (data not shown). Basal respiration was calculated as the last rate measurement before oligomycin injection minus non-mitochondrial QO_2 after AA/R addition. ATP-linked respiration was calculated as the difference between basal respiration and the minimum rate measurement after oligomycin injection. Spare respiratory capacity is the maximal respiration rate (maximal rate after FCCP injection minus non- mitochondrial respiration) minus basal respiration rate. Coupling efficiency was calculated as the ratio of ATP-linked respiration with the basal respiration rate × 100. The cell respiratory control ratio (RCR) was calculated as the ratio of the uncoupled rate to the oligomycin rate (analogous to state 3/state 4 in isolated mitochondria).

Measurement of mitochondrial membrane potential ($\Delta\Psi_m$).

Mitochondrial membrane potential ($\Delta\Psi_m$) was assessed using the aggregate-forming lipophilic cationic probe fluorochrome JC-1 (87). In the presence of physiological mitochondrial membrane potentials, JC-1 forms aggregates that fluoresce with an emission peak at 590 nm (red). Disruption or loss of membrane potential favors the monomeric form of JC-1, which has an emission peak at 525 nm (green). To examine the effect of MnP on modifications induced by SIN-1, BAEC were grown in 6-well culture plates in M199 with 10 % FBS, once they reached 90% confluence, the medium was changed to 0.4 % FBS for 12 h, and incubated with Mn(III)TnBuOE-2-PyP^{5+} (5 μM) for 2 hours to allow incorporation into the mitochondria. Then, cells were washed twice and exposed to SIN-1 (100 μM) overnight in M199 with 0.4 % FBS. JC-1 (2 μM) was added and incubated for 20 min at 37 °C and rinsed with Krebs buffer. Mitochondrial membrane potential was inferred from the ratio of fluorescence intensity JC-1 aggregate/monomer. The images were acquired from randomly chosen fields using an inverted epifluorescence microscope (Olympus IX70).

Flow cytometric evaluation of apoptosis.

To evaluate the effect of MnP on the apoptotic cell death induction by SIN-1, BAEC were pretreated with Mn(III)TnBuOE-2-PyP^{5+} (5 μM) for 2 h, washed twice, and incubated overnight with SIN-1 (250 μM). Then, cells were washed with PBS, harvested by trypsinization, labeled with Annexin-V-FITC or Alexa Fluor 488 anti BrDU antibody and analyzed by flow cytometry BD FACSCalibur apparatus (Becton Dickinson), at least 10,000 events of total cells were analyzed by each experimental treatment. Results are expressed as the percentage of Annexin-V positive cells with

respect to the total cell count (1 x 10^4 cells were considered as 100 %) in each condition. Apoptotic cells labeling was determined by the mean sample fluorescence intensity/control fluorescence intensity, expressed in arbitrary units. As control, in order to confirm the nature of cell death, necrosis was evaluated by propidium iodide (PI) staining, following the same procedure as described before with Annexin-V. Furthermore, we also verified that pretreatment with MnP did not induce appreciable cell death as assayed either by apoptosis or necrosis by flow cytometry (data not shown).

Data analysis.

All experiments reported herein were reproduced at least three times, and results shown correspond to one representative experiment of each one unless otherwise indicated. All data are given as means ± SD or SEM unless otherwise noted, and $P < 0.05$ was considered significant. Statistical significance in cell experiments was determined using one-way ANOVA followed by *t*-test unpaired with Welch´s correction for comparisons among multiple groups. RR spectra analysis was performed using homemade software that allows for baseline subtraction and iterative convolution. Semi-quantification of the relative concentrations was achieved by integration of the ν_4 band. The RR relative cross-sections for the reduced and oxidized species were obtained from the reduced Mn(II)P and oxidized Mn(III)P spectra obtained by mixing with excess sodium dithionite or potassium ferricyanide, respectively. Graphics and mathematical fits to experimental data were performed using OriginPro 8 (OriginLab Corporation) or GraphPad Prism version 6.0.

RESULTS

RR spectra of MnP.

The high frequency RR spectra of porphyrins (ca. 1300-1700 cm^{-1}) are dominated by skeletal modes that are sensitive to the macrocycle core size and electron density and thus, constitute characteristic marker bands of the oxidation state, spin and axial coordination of the central metal ion (88-91). First, we characterized the RR spectra of MnTnHex-2-PyP^{5+} and MnTnBuOE-2-PyP^{5+} in PBS buffer solution. As shown in Figure 1A, the RR spectra of both MnP were quite similar to each other in terms of band positions and relative intensities, both in the oxidized Mn(III)P and dithionite-reduced Mn(II)P states. In the Mn(III) form, MnTnHex-2-PyP^{5+} and MnTnBuOE-2-PyP^{5+} showed bands at 1258, 1370 and 1570 cm^{-1}, in agreement with the porphyrin-core sensitive vibrations reported before for metalloporphyrins, and can be assigned based on previous work on manganese(III) tetrakis(4-sulfophenyl)porphyrin (MnTPP-PyP) and manganese(III) tetrakis(1-methylpyridinium-4-yl)porphyrin (MnTM-4-PyP^{5+}) to: δ (C_m – pyr), ν_s (C_α - N) and ν_s (C_β - C_β), respectively (88,92). Upon reduction with excess dithionite, we observed for both MnP the characteristic downshift of the 1370 and 1570 cm^{-1} bands to 1347 and 1550 cm^{-1}, respectively, in agreement with previous reports (92), as well as the rise of a new band at 1440 cm^{-1} and a gain of intensity for the band centered at 1258 cm^{-1} (Figure 1A). As control, the initial RR spectra of Mn(III)P were completely recovered after addition of excess potassium ferricyanide to Mn(II)P (data not shown). In addition, as shown in Figure 1B, RR spectra of Mn(III)P did not appreciably change in the presence of the peroxynitrite donor SIN-1. However, when Mn(III)P was first reduced by ascorbic acid and then treated with SIN-1, we observed a change in the RR bands consistent to the oxidation of Mn(II)P to Mn(III)P, with no evidence for other Mn redox states or complexes such as the formation of a metal-

nitrosyl complex form the reaction between the reduced MnP, Mn(II)TE-2-PyP^{5+} with $^{\bullet}$NO (93).

These experiments confirm that RR spectroscopy is a sensitive and useful method to assign the redox state of the two porphyrins studied here, and that the ν_s (C_α - N) band is an optimal spectral indicator because of the 23 cm^{-1} shift between redox states and its high intensity in a spectrally clean region. It is important to remark that experimental RR conditions such as laser wavelength, laser power at sample, rotational speed of the cuvette and exposure times, were carefully controlled and optimized in order to avoid photoreduction or any other laser-induce damage of the MnP.

Intramitochondrial redox state of MnP studied by RR.

As reported previously, Mn(III)P can be readily reduced by intracellular components, in particular by the Complexes I and II of the mitochondrial electron transport chain (16-18).Thus, we next attempted to directly assess the redox state of MnP incubated with intact isolated mitochondria by RR confocal microscopy. As expected, when Mn(III)TnHex-2-PyP^{5+} was added to mitochondria in the absence of an electron source as substrate, RR spectra showed bands at 1370 and 1570 cm^{-1}, corresponding to the oxidized Mn(III)P (Figure 2c). Upon addition of succinate as a metabolic substrate of Complex II, we observed an intensity drop of the bands at 1370 cm^{-1} and 1570 cm^{-1}, concomitant with the rise of bands at 1347 and 1550 cm^{-1}, which is consistent with the reduction to Mn(II)TnHex-2-PyP^{5+} (Figure 2d). From the integration of the two bands and the relative RR cross-sections of the porphyrin in the two redox states, as obtained from spectra of chemically reduced and oxidized samples, we determined that > 70 % of the incorporated porphyrin was reduced under these conditions. Control experiments showed that succinate was not able to reduce the Mn(III)P in the absence of

mitochondria (Figure 2b). In order to confirm the reduction by mitochondrial components, we performed control experiments with the addition of compounds that selectively inhibit electron transfer at different points of the mitochondrial respiratory chain. When isolated mitochondria were incubated in the presence of succinate as electron source and of antimycin A as inhibitor of the respiratory Complex III, the measured RR spectrum was dominated by an intense band at 1347 cm^{-1} and a weaker band at 1370 cm^{-1}, which after quantification revealed that *ca.* 80% of the incorporated Mn(III)TnHex-2-PyP^{5+} was effectively reduced by mitochondrial components (Figure 2f). For incubations in the presence of rotenone and malonate, inhibitors of Complexes I and II, respectively, the intensity ratio of the 1347 and 1370 cm^{-1} bands was reversed (Figure 2e), which indicates that the reduction of MnP was significantly hindered under these conditions to only *ca.* 36%. Next, we investigated the redox state of MnTnBuOE-2-PyP^{5+} in mitochondria exposed to SIN-1. As observed before, in presence of succinate, the RR spectra indicate that MnP was mostly in the reduced state (Figure 3A, c). When SIN-1 was added, RR bands did not change appreciably and corresponded predominantly to the Mn(II)P state, indicating that the levels of succinate readily restored the oxidative effects of SIN-1 (Figure 3A, d). This is important since, according to the catalytic cycle (eq. 1-3), the antioxidant protection is effective as long as MnP is reduced faster than it is oxidized, keeping high steady-state levels of Mn(II)P. Nevertheless, in the presence of the inhibitors rotenone and thenoyl trifluoroacetate (TTFA), when cells were exposed SIN-1, the intensity ratio of the RR bands of MnP at 1347 and 1370 cm^{-1} was reversed, indicating that MnP mainly evolved to the oxidized state (Figure 3B, c and d).

Incorporation and redox state of MnP in BAEC studied by RR.

In order to evaluate the uptake of MnP in living cells by RR spectroscopy, a confluent BAEC culture was preincubated with Mn(III)TnBuOE-2-PyP^{5+} or Mn(III)TnHex-2-PyP^{5+} for 2 h. After treatment, the cells were extensively washed with PBS buffer prior to RR measurements in order to remove remaining free MnP and also to eliminate potential artifacts produced by residues of the culture medium. As shown in Figure 4b, the RR spectra of cells incubated with Mn(III)TnHex-2-PyP^{5+} display a band at 1347 cm^{-1}. The position and relative intensity of the ν_s (C_α - N) RR band argues in favor of MnP existing predominantly in the reduced state when incorporated into living cells. Similar results were obtained with Mn(III)TnBuOE-2-PyP^{5+} (data not shown). It is remarkable that RR signals of MnP could be detected above the scattering background of cellular components. Next, we studied the redox state of MnP in BAEC challenged by SIN-1. In this case, cells were resuspended in PBS and Mn(III)TnHex-2-PyP^{5+} was added directly to the sample. As expected, we obtained a similar result than with isolated mitochondria. RR spectra showed that when succinate was added to the cells, MnP was mostly reduced to Mn(II)P (Figure 5c); when SIN-1 was added in the presence of rotenone and TTFA, a time-dependent oxidation to Mn(III)P was observed, as indicated by the shift of the RR bands, particularly the change from 1347 to 1370 cm^{-1} (Figure 5, e and f).

Reaction of Mn(III)TnBuOE-2-PyP^{5+} with peroxynitrite. The kinetics of Mn(III)TnBuOE-2-PyP^{5+} reaction with excess peroxynitrite were measured through stopped-flow spectrophotometry. The decay of Mn(III)TnBuOE-2-PyP^{5+} followed exponential functions (Figure 6A) and the observed pseudo-first order rate constants (k_{obs}) increased linearly with peroxynitrite concentrations (Figure 6B). From the slope of the plot, the apparent second-order rate constant (k_{app}) was determined to be (3.5 ± 0.1)

x 10^7 M^{-1} s^{-1} at pH 7.2 and 37 °C. To study the pH-dependence of the reaction kinetics, the apparent second-order rate constants of Mn(III)TnBuOE-2-PyP^{5+} oxidation by peroxynitrite were determined from the slope of plots of k_{obs} versus peroxynitrite concentrations at different pHs in the range of 5.23 to 7.20. As shown in Figure 6C, there is a sigmoideal dependence of k_{app} with pH, with an inflection point at pH ~ 6.29 and reaches maximal values al pH ≥ 7. Given that the pK_a of ONOOH is 6.75 (94), this behavior is consistent with Mn(III)P reacting fast with $ONOO^-$, and much more slowly with ONOOH, as reported for all the MnP previously studied (8,9).

Effect of MnP on cell-derived peroxynitrite in endothelial cells.

In order to obtain more evidence of the subcellular distribution and the effect of MnP in mitochondria, we evaluated their influence on endogenous mitochondrial peroxynitrite formation. The specific and sensitive detection of peroxynitrite generation in BAEC was monitored using the fluorescein-boronate probe (Fl-B), which reacts fast with peroxynitrite with a rate constant of k = 1.7 x 10^6 M^{-1} s^{-1}, several orders of magnitude greater than for hydrogen peroxide (1.7 M^{-1} s^{-1}) (74). BAEC were stimulated to produce mitochondrial $O_2^{\bullet-}$ by the use of antimycin A, and intramitochondrial peroxynitrite was generated in the presence of a $^{\bullet}NO$ donor (NOC-7). As shown in Figure 7, when BAEC were exposed to the combination of antimycin A and NOC-7, a maximal increase in fluorescence intensity over time corresponding to Fl-B oxidation was observed, indicating peroxynitrite generation. Remarkably, in the presence of MnTnBuOE-2-PyP^{5+}, FI-B oxidation was partially inhibited (~ 40%). To note, the small fluorescence signal obtained with NOC-7 alone is expected based on the known stimulation of mitochondrial-$O_2^{\bullet-}$ and consequently peroxynitrite, secondary to the $^{\bullet}NO$-mediated inhibition of cytochrome c oxidase (83,95,96).

Peroxynitrite-induced mitochondrial dysfunction is partially prevented by MnP.

Mitochondrial function was studied by measuring the oxygen consumption rates (QO_2) in cells pre-treated with Mn(III)TnBuOE-2-PyP^{5+} and exposed to exogenous flux of peroxynitrite generated by SIN-1. A representative time course of cell respiratory control experiments is shown in Figure 8A. First, QO_2 was measured under basal conditions, followed by the sequential addition of an inhibitor of ATP synthase, oligomycin (1 μM), a proton ionophore, FCCP (1 μM), and a mixture of electron transport chain inhibitors, rotenone/antimycin A (1 μM/0.1 μM), as indicated. A remarkable protection effect of MnTnBuOE-2-PyP^{5+} on oxygen consumption profile was evident along the assay when compared to SIN-1-exposed cells in the absence of MnP (Figure 8A). In order to evaluate major aspects of mitochondrial function, key parameters were calculated as described in experimental procedures section. Basal respiration (before addition of reagents), ATP-linked respiration and spare respiratory capacity were all impaired by SIN-1 treatment compared with control cells in the absence of SIN-1. All these effects were significantly restored when BAEC were preincubated with Mn(III)TnBuOE-2-PyP^{5+}, supporting the protective effect of MnP against the peroxynitrite-induced damage in mitochondria (Figure 8, B-D). Furthermore, to evaluate the ability of mitochondria to couple oxygen consumption to oxidative phosphorylation, respiratory control ratios (RCR) were also determined. RCR is a particularly revealing parameter to assess mitochondrial function since it reflects the tight coupling between respiration and oxidative phosphorylation. As shown in Figure 8E, RCR was significantly reduced by SIN-1 whereas preincubation with Mn(III)TnBuOE-2-PyP^{5+} partially avoided this effect.

Protective effect of MnP on mitochondrial membrane potential ($\Delta\Psi_m$) exposed to SIN-1.

Mitochondrial membrane potential ($\Delta\Psi_m$) was assessed using the fluorescent probe JC-1. When subjected to physiological mitochondrial membrane potentials, JC-1 forms aggregates that fluoresce with an emission peak at 590 nm (red). Loss of membrane potential favors the monomeric form of JC-1, which presents an emission peak at 525 nm (green). As shown in Figure 9, exposure to SIN-1 (100 μM) disrupts the $\Delta\Psi_m$, as indicated by an increase in the monomeric JC-1 fraction (decrease in the red/green ratio fluorescent). In agreement with cell respiratory results, the disruption on $\Delta\Psi_m$ induced by SIN-1 was prevented by preincubation with Mn(III)TnBuOE-2-PyP^{5+}. Similar results were obtained upon exposure to SIN-1 (250 μM) and using Mn(III)TnHex-2-PyP^{5+} (data not shown).

Effect of MnP on apoptosis triggered by SIN-1 in BAEC.

As observed before, SIN-1 affects mitochondrial function and disrupts $\Delta\Psi_m$, events that can lead to activation of apoptotic cell death (78,82). Moreover, mitochondria-derived reactive species have been associated with the initiation phase of the apoptotic cell death (97,98). In order to evaluate the effect of MnP on apoptosis induced by SIN-1 on BAEC, we measured the exposure of phosphatidylserine (PS) by anexin-V FITC by flow cytometry analysis. As shown in Figure 10, SIN-1 induced an increase in PS externalization and pretreatment with Mn(III)TnBuOE-2-PyP^{5+} significantly reduced the amount of apoptotic cells induced by SIN-1. As control, we did not observe significant differences with respect to the untreated cells in the percentage of PI-positive cells when BAEC was exposed to SIN-1 (data not shown), ruling out a necrotic cell death and supporting an apoptotic pathway induced by peroxynitrite, as reported

previously (97,99). Thus, MnTnBuOE-2-PyP^{5+} protect BAEC against nitroxidative damage, maintaining the mitochondrial function, integrity and promoting cell survival.

DISCUSSION

In the present study, we introduced the application of RR spectroscopy as an effective tool for the direct and noninvasive evaluation of the uptake and redox state of MnP in living cells. First, we characterized the RR spectra of two cationic MnP, MnTnBuOE-2-PyP^{5+} and MnTnHex-2-PyP^{5+} both as Mn(III) and Mn(II) complexes (Figure 1), and identified the porphyrin marker bands based on previous vibrational assignments (88,92). MnP redox state was also assayed by RR spectroscopy in isolated mitochondria, which can readily reduce Mn(III) to Mn(II). Addition of SIN-1, in the presence of compounds that selectively inhibit the electron transport chain, resulted in substantial changes in the RR spectra of MnP, with a time-dependent oxidation of Mn(II)P to Mn(III)P (Figures 3 and 5).

These assays provide additional evidence of the known contribution of mitochondrial components on MnP reduction. Furthermore, the RR experiments confirm that Mn(III)P are effectively incorporated and accumulated in endothelial cells and reduced by intracellular components (Figure 3). It is remarkable that MnP can be detected by RR spectroscopy in a cell system, even when BAEC were incubated with low micromolar concentrations of Mn(III)P (5 μM). Together these results support RR spectroscopy as a suitable approach to assess incorporation and intracellular redox speciation of MnP in biological systems. The method is capable of providing important new insights to unravel antioxidant action mechanisms in living cells and, if coupled to confocal

microscopy, this information can potentially be obtained with subcellular spatial resolution.

The ability of MnP to scavenge reactive species and act as an efficient antioxidant in biological systems would depend on kinetic factors, such as the rate constant and concentration in cell compartments. In this sense, we characterized the kinetics of the peroxynitrite reaction with Mn(III)TnBuOE-2-PyP^{5+} (Figure 6). The second-order rate constant was determined to be (3.5 ± 0.1) x 10^7 M^{-1} s^{-1} at pH 7.2 and 37 °C, which is in the range of the previously reported rate constants of peroxynitrite reduction by other cationic Mn(III)P, and is similar to the reported value for Mn(III)TnHex-2-PyP^{5+} (1.3 x 10^7 M^{-1} s^{-1}) (8,14). Also, the pH-dependent study shows that the reaction rate of Mn(III)TnBuOE-2-PyP^{5+} is faster with $ONOO^-$ than with ONOOH, as expected due to the electrostatic facilitation of former reaction between species of opposite charges and as earlier seen in reaction between other cathionic MnP and $O_2^{\bullet-}$ or $ONOO^-$(8,13). Mn(II)P can react fast and efficiently with peroxynitrite, as reported for Mn(II)TE-2-PyP^{5+} with a rate constant > 10^7 M^{-1} s^{-1} (eq. 3) (17). This is relevant considering that the initial Mn(III) complex can be reduced to Mn(II) by intracellular reductants and Mn(II) is the predominant oxidation state of intracellular MnP, as confirmed herein by RR spectroscopy studies. Based on these relatively high rate constants, it can be concluded that direct reactions with peroxynitrite are fast enough to outcompete peroxynitrite-dependent oxidant reactions with cellular targets and allows us to rationalize a role as an antioxidant in biological systems. In addition, pharmacokinetic studies performed with MnTE-2-PyP^{5+} in mouse, reported a concentration of 5.1 μM in heart mitochondria up to 7 h after a single intraperitoneal administration of 10 mg/kg of the compound. Taking into account the reported lower limit rate constant of Mn(II)TE-2-PyP^{5+}, the value

k_{app}[T] (product of the rate constant and target concentration) was estimated in the range for a suitable peroxynitrite scavenger to be competitive (17,58,100). Therefore, MnP can be effective antioxidants to protect from peroxynitrite-mediated damage to mitochondria (17,101) and cells (this paper), provided that they can be reduced to the Mn(II) state. As long as the redox metabolism keeps the MnP in the reduced state, the compound will be an efficient neutralizer of the cytotoxic effects of peroxynitrite; of course, if intracellular redox conditions change in a way that increasing amounts of Mn(III)P arise (e.g. sustained oxidative stress, depletion or disruption of reducing systems), then the protective antioxidant actions of MnP will progressively decline due to, among other factors, the secondary formation of $^{\bullet}NO_2$ (Eq. 1-3). Theoretically, MnP could also attenuate SIN-1-dependent toxicity by scavenging of $O_2^{\bullet-}$ or trapping of $^{\bullet}NO$; the first mechanism is ruled out based on kinetic grounds as intracellular SOD levels would be at least 1,000 fold more efficient than micromolar MnP concentrations used herein (3-6). The second mechanism involving the formation of Mn(II)P-nitrosyl complexes is also not kinetically favored as the rate constant of $^{\bullet}NO$ with Mn(II)P is at least one order of magnitude lower than that for peroxynitrite (93) and it is an stoichiometric process which can not account for the protection observed against a large excess of SIN-1.

Several studies have evidenced the formation of mitochondria-derived oxidants and peroxynitrite formation, leading to nitro-oxidative modification of mitochondrial components, related to different pathological conditions (20,24,29,101). Thus, it is important to confirm the preferential subcellular distribution of MnP and its colocalization, since mitochondria are the site where most of the oxidants can be formed and where MnP could exert their function as catalytic antioxidants. The fact that MnP inhibited intra-mitochondrial Fl-B oxidation by peroxynitrite strongly supports its site-

specific protective role in mitochondria (Figure 7). In addition, we evaluated the protective capacity of MnP on mitochondrial integrity and functionality by exposing the endothelial cells to nitro-oxidative stress induced by the peroxynitrite donor SIN-1. First, we assessed the functional profile through oxygen consumption rates measurements (Figure 8). Our results show that MnTnBuOE-2-PyP^{5+} was capable to largely protect against peroxynitrite-mediated mitochondrial dysfunction in BAEC by avoiding the impairment of different functional parameters: basal, ATP-linked cellular respiration, spare respiratory capacity and RCR. In line with these mitochondrial functional results, pretreatment with Mn(III)P was effective in protecting BAEC from peroxynitrite-induced loss of mitochondrial membrane integrity, as shown by preserving the mitochondrial membrane potential ($\Delta\Psi_m$) (Figure 9), and preventing apoptotic cell death (Figure 10). These results are in full agreement with previous reports with submitochondrial particles (SMP), in which MnTE-2-PyP^{5+} was able to protect the succinate dehydrogenase and succinate oxidase activities of mitochondrial electron transport chain from peroxynitrite-mediated damage (17). In addition, MnP also protected SMP from peroxynitrite-dependent inactivation of NADH dehydrogenase activity and inhibition of complex I-dependent oxygen consumption, protein radical and nitrotyrosine formation (101). Remarkably, the observed protection by MnP was obtained at low micromolar concentration (cells were treated with 5 μM Mn(III)P), which is compatible with the levels detected by RR spectroscopy in BAEC and correspond to the reported levels achievable in mitochondria *in vivo* (58).

Overall, the data presented herein provide the basis for the application of RR spectroscopy as a valuable methodology that allows observing the intracellular accumulation of the MnP and monitoring their redox state in cell culture systems. RR

results confirmed that Mn(III)P are effectively incorporated into endothelial cells and can be reduced by intracellular components, in particular those of the mitochondrial electron transport chain. Also, MnP protected endothelial cells from peroxynitrite-mediated nitro-oxidative damage, preserving mitochondrial function and preventing apoptosis. The combined studies of redox interactions and reactivity of MnP presented herein add new elements to understand their mechanisms of antioxidant capacity in biological systems.

ACKNOWLEDGMENTS

This work was supported by grants and fellowships from Universidad de la República (CSIC, to S. C., V. V and R. R.), AUGM (to S. C.), CeBEM (to S. C. and V. V.), ANPCyT and UBACYT (to D.H.M). We thank Dr. Adalí Pecci and Dr. Jimena Martínez for technical assistance on cell culture at Facultad de Ciencias Exactas y Naturales, UBA. We thank Natalia Ríos for the synthesis of Fl-B and technical assistance, and Drs. Adrian Aicardo, Lucía Piacenza and Alejandra Martínez for helpful discussions.

Funding Sources: This work was supported by grants and fellowships from: Universidad de la República (CSIC and Espacio Interdisciplinario), AUGM, CeBEM, PEDECIBA, Agencia Nacional de Investigación e Innovación (ANII), ANPCyT and UBACYT. DAP and DHM are staff members of CONICET.

REFERENCES

1. Archibald, F. S., and Fridovich, I. (1982) The scavenging of superoxide radical by manganous complexes: in vitro. *Arch Biochem Biophys* **214**, 452-463
2. Batinic-Haberle, I., Liochev, S. I., Spasojevic, I., and Fridovich, I. (1997) A potent superoxide dismutase mimic: manganese beta-octabromo-meso-tetrakis-(N-methylpyridinium-4-yl) porphyrin. *Arch Biochem Biophys* **343**, 225-233
3. Batinic-Haberle, I. (2002) Manganese porphyrins and related compounds as mimics of superoxide dismutase. *Methods Enzymol* **349**, 223-233
4. Batinic-Haberle, I., Spasojević, I., Hambright, P., Benov, L., Crumbliss, A. L., and Fridovich, I. (1999) Relationship among Redox Potentials, Proton Dissociation Constants of Pyrrolic Nitrogens, and in Vivo and in Vitro Superoxide Dismutating Activities of Manganese(III) and Iron(III) Water-Soluble Porphyrins. *Inorg Chem* **38**, 4011-4022
5. Batinic-Haberle, I., Spasojevic, I., Stevens, R. D., Hambright, P., Neta, P., Okado-Matsumoto, A., and Fridovich, I. (2004) New class of potent catalysts of O2.-dismutation. Mn(III) ortho-methoxyethylpyridyl- and di-ortho-methoxyethylimidazolylporphyrins. *Dalton Trans* 1696-1702
6. Faulkner, K. M., Liochev, S. I., and Fridovich, I. (1994) Stable Mn(III) porphyrins mimic superoxide dismutase in vitro and substitute for it in vivo. *J Biol Chem* **269**, 23471-23476
7. Day, B. J., Fridovich, I., and Crapo, J. D. (1997) Manganic porphyrins possess catalase activity and protect endothelial cells against hydrogen peroxide-mediated injury. *Arch Biochem Biophys* **347**, 256-262
8. Ferrer-Sueta, G., Vitturi, D., Batinic-Haberle, I., Fridovich, I., Goldstein, S., Czapski, G., and Radi, R. (2003) Reactions of manganese porphyrins with peroxynitrite and carbonate radical anion. *J Biol Chem* **278**, 27432-27438
9. Ferrer-Sueta, G., Batinic-Haberle, I., Spasojevic, I., Fridovich, I., and Radi, R. (1999) Catalytic scavenging of peroxynitrite by isomeric Mn(III) N-methylpyridylporphyrins in the presence of reductants. *Chem Res Toxicol* **12**, 442-449
10. Ferrer-Sueta, G., Ruiz-Ramirez, L., and Radi, R. (1997) Ternary copper complexes and manganese (III) tetrakis(4-benzoic acid) porphyrin catalyze peroxynitrite-dependent nitration of aromatics. *Chem Res Toxicol* **10**, 1338-1344
11. Groves, J. T., and Marla, S. S. (1995) Peroxynitrite-induced DNA strand scission mediated by a manganese porphyrin. *Journal of the American Chemical Society* **117**, 9578-9579
12. Lee, J., Hunt, J., and Groves, J. T. (1997) Rapid decomposition of peroxynitrite by manganese porphyrin-antioxidant redox couples. *Bioorg Med Chem Lett* **7**, 2913-2918
13. Spasojevic, I., Batinic-Haberle, I., Reboucas, J. S., Idemori, Y. M., and Fridovich, I. (2003) Electrostatic contribution in the catalysis of O2*-dismutation by superoxide dismutase mimics. MnIIITE-2-PyP5+ versus MnIIIBr8T-2-PyP+. *J Biol Chem* **278**, 6831-6837
14. Tovmasyan, A., Carballal, S., Ghazaryan, R., Melikyan, L., Weitner, T., Maia, C. G., Reboucas, J. S., Radi, R., Spasojevic, I., Benov, L., and Batinic-Haberle, I. (2014) Rational design of superoxide dismutase (SOD) mimics: the evaluation

of the therapeutic potential of new cationic Mn porphyrins with linear and cyclic substituents. *Inorg Chem* **53**, 11467-11483

15. Trostchansky, A., Ferrer-Sueta, G., Batthyany, C., Botti, H., Batinic-Haberle, I., Radi, R., and Rubbo, H. (2003) Peroxynitrite flux-mediated LDL oxidation is inhibited by manganese porphyrins in the presence of uric acid. *Free Radic Biol Med* **35**, 1293-1300
16. Batinic-Haberle, I., Spasojevic, I., and Fridovich, I. (2004) Tetrahydrobiopterin rapidly reduces the SOD mimic Mn(III) ortho-tetrakis(N-ethylpyridinium-2-yl)porphyrin. *Free Radic Biol Med* **37**, 367-374
17. Ferrer-Sueta, G., Hannibal, L., Batinic-Haberle, I., and Radi, R. (2006) Reduction of manganese porphyrins by flavoenzymes and submitochondrial particles: a catalytic cycle for the reduction of peroxynitrite. *Free Radic Biol Med* **41**, 503-512
18. Kachadourian, R., Johnson, C. A., Min, E., Spasojevic, I., and Day, B. J. (2004) Flavin-dependent antioxidant properties of a new series of meso-N,N'-dialkyl-imidazolium substituted manganese(III) porphyrins. *Biochem Pharmacol* **67**, 77-85
19. Quijano, C., Trujillo, M., Castro, L., and Trostchansky, A. (2016) Interplay between oxidant species and energy metabolism. *Redox Biol* **8**, 28-42
20. Radi, R., Cassina, A., Hodara, R., Quijano, C., and Castro, L. (2002) Peroxynitrite reactions and formation in mitochondria. *Free Radic Biol Med* **33**, 1451-1464
21. Hsu, J. L., Hsieh, Y., Tu, C., O'Connor, D., Nick, H. S., and Silverman, D. N. (1996) Catalytic properties of human manganese superoxide dismutase. *J Biol Chem* **271**, 17687-17691
22. Knoops, B., Goemaere, J., Van der Eecken, V., and Declercq, J. P. (2011) Peroxiredoxin 5: structure, mechanism, and function of the mammalian atypical 2-Cys peroxiredoxin. *Antioxid Redox Signal* **15**, 817-829
23. Trujillo, M., Clippe, A., Manta, B., Ferrer-Sueta, G., Smeets, A., Declercq, J. P., Knoops, B., and Radi, R. (2007) Pre-steady state kinetic characterization of human peroxiredoxin 5: taking advantage of Trp84 fluorescence increase upon oxidation. *Arch Biochem Biophys* **467**, 95-106
24. Castro, L., Demicheli, V., Tortora, V., and Radi, R. (2011) Mitochondrial protein tyrosine nitration. *Free Radic Res* **45**, 37-52
25. Poderoso, J. J., Carreras, M. C., Lisdero, C., Riobo, N., Schopfer, F., and Boveris, A. (1996) Nitric oxide inhibits electron transfer and increases superoxide radical production in rat heart mitochondria and submitochondrial particles. *Arch Biochem Biophys* **328**, 85-92
26. Radi, R., Rodriguez, M., Castro, L., and Telleri, R. (1994) Inhibition of mitochondrial electron transport by peroxynitrite. *Arch Biochem Biophys* **308**, 89-95
27. de Cavanagh, E. M., Inserra, F., Ferder, M., and Ferder, L. (2007) From mitochondria to disease: role of the renin-angiotensin system. *Am J Nephrol* **27**, 545-553
28. Federico, A., Cardaioli, E., Da Pozzo, P., Formichi, P., Gallus, G. N., and Radi, E. (2012) Mitochondria, oxidative stress and neurodegeneration. *J Neurol Sci* **322**, 254-262
29. Ghafourifar, P., Schenk, U., Klein, S. D., and Richter, C. (1999) Mitochondrial nitric-oxide synthase stimulation causes cytochrome c release from isolated

mitochondria. Evidence for intramitochondrial peroxynitrite formation. *J Biol Chem* **274**, 31185-31188

30. Newsholme, P., Gaudel, C., and Krause, M. (2012) Mitochondria and diabetes. An intriguing pathogenetic role. *Adv Exp Med Biol* **942**, 235-247
31. Nicolson, G. L. (2007) Metabolic syndrome and mitochondrial function: molecular replacement and antioxidant supplements to prevent membrane peroxidation and restore mitochondrial function. *J Cell Biochem* **100**, 1352-1369
32. Szabo, C., Ischiropoulos, H., and Radi, R. (2007) Peroxynitrite: biochemistry, pathophysiology and development of therapeutics. *Nat Rev Drug Discov* **6**, 662-680
33. Cassina, P., Cassina, A., Pehar, M., Castellanos, R., Gandelman, M., de Leon, A., Robinson, K. M., Mason, R. P., Beckman, J. S., Barbeito, L., and Radi, R. (2008) Mitochondrial dysfunction in SOD1G93A-bearing astrocytes promotes motor neuron degeneration: prevention by mitochondrial-targeted antioxidants. *J Neurosci* **28**, 4115-4122
34. Hachmeister, J. E., Valluru, L., Bao, F., and Liu, D. (2006) Mn (III) tetrakis (4-benzoic acid) porphyrin administered into the intrathecal space reduces oxidative damage and neuron death after spinal cord injury: a comparison with methylprednisolone. *J Neurotrauma* **23**, 1766-1778
35. Nin, N., Cassina, A., Boggia, J., Alfonso, E., Botti, H., Peluffo, G., Trostchansky, A., Batthyany, C., Radi, R., Rubbo, H., and Hurtado, F. J. (2004) Septic diaphragmatic dysfunction is prevented by Mn(III)porphyrin therapy and inducible nitric oxide synthase inhibition. *Intensive Care Med* **30**, 2271-2278
36. Batinic-Haberle, I., Tovmasyan, A., and Spasojevic, I. (2015) An educational overview of the chemistry, biochemistry and therapeutic aspects of Mn porphyrins--From superoxide dismutation to H2O2-driven pathways. *Redox Biol* **5**, 43-65
37. Batinic-Haberle, I., and Spasojevic, I. (2014) Complex chemistry and biology of redox-active compounds, commonly known as SOD mimics, affect their therapeutic effects. *Antioxid Redox Signal* **20**, 2323-2325
38. Batinic-Haberle, I., Rajic, Z., Tovmasyan, A., Reboucas, J. S., Ye, X., Leong, K. W., Dewhirst, M. W., Vujaskovic, Z., Benov, L., and Spasojevic, I. (2011) Diverse functions of cationic Mn(III) N-substituted pyridylporphyrins, recognized as SOD mimics. *Free Radic Biol Med* **51**, 1035-1053
39. Batinic-Haberle, I., Reboucas, J. S., and Spasojevic, I. (2010) Superoxide dismutase mimics: chemistry, pharmacology, and therapeutic potential. *Antioxid Redox Signal* **13**, 877-918
40. Batinic-Haberle, I., Spasojevic, I., Stevens, R. D., Hambright, P., and Fridovich, I. (2002) Manganese (III) meso-tetrakis (ortho-N-alkylpyridyl) porphyrins. Synthesis, characterization, and catalysis of O 2â˙’ dismutation. *Journal of the Chemical Society, Dalton Transactions* 2689-2696
41. Cline, J. M., Dugan, G., Bourland, J. D., Perry, D. L., Stitzel, J. D., Weaver, A. A., Jiang, C., Tovmasyan, A., Owzar, K., Spasojevic, I., Batinic-Haberle, I., and Vujaskovic, Z. (2018) Post-Irradiation Treatment with a Superoxide Dismutase Mimic, MnTnHex-2-PyP(5+), Mitigates Radiation Injury in the Lungs of Non-Human Primates after Whole-Thorax Exposure to Ionizing Radiation. *Antioxidants (Basel)* **7**,
42. Sheng, H., Spasojevic, I., Tse, H. M., Jung, J. Y., Hong, J., Zhang, Z., Piganelli, J. D., Batinic-Haberle, I., and Warner, D. S. (2011) Neuroprotective efficacy from a lipophilic redox-modulating Mn(III) N-Hexylpyridylporphyrin,

MnTnHex-2-PyP: rodent models of ischemic stroke and subarachnoid hemorrhage. *J Pharmacol Exp Ther* **338**, 906-916

43. Rajic, Z., Tovmasyan, A., Spasojevic, I., Sheng, H., Lu, M., Li, A. M., Gralla, E. B., Warner, D. S., Benov, L., and Batinic-Haberle, I. (2012) A new SOD mimic, Mn(III) ortho N-butoxyethylpyridylporphyrin, combines superb potency and lipophilicity with low toxicity. *Free Radic Biol Med* **52**, 1828-1834
44. Rajic, Z., Tovmasyan, A., de Santana, O. L., Peixoto, I. N., Spasojevic, I., do Monte, S. A., Ventura, E., Reboucas, J. S., and Batinic-Haberle, I. (2017) Challenges encountered during development of Mn porphyrin-based, potent redox-active drug and superoxide dismutase mimic, MnTnBuOE-2-PyP(5+), and its alkoxyalkyl analogues. *J Inorg Biochem* **169**, 50-60
45. Zhao, Y., Carroll, D. W., You, Y., Chaiswing, L., Wen, R., Batinic-Haberle, I., Bondada, S., Liang, Y., and St Clair, D. K. (2017) A novel redox regulator, MnTnBuOE-2-PyP(5+), enhances normal hematopoietic stem/progenitor cell function. *Redox Biol* **12**, 129-138
46. Bakthavatchalu, V., Dey, S., Xu, Y., Noel, T., Jungsuwadee, P., Holley, A. K., Dhar, S. K., Batinic-Haberle, I., and St Clair, D. K. (2012) Manganese superoxide dismutase is a mitochondrial fidelity protein that protects Polgamma against UV-induced inactivation. *Oncogene* **31**, 2129-2139
47. Batinic-Haberle, I., Tovmasyan, A., Roberts, E. R., Vujaskovic, Z., Leong, K. W., and Spasojevic, I. (2014) SOD therapeutics: latest insights into their structure-activity relationships and impact on the cellular redox-based signaling pathways. *Antioxid Redox Signal* **20**, 2372-2415
48. Miriyala, S., Thippakorn, C., Chaiswing, L., Xu, Y., Noel, T., Tovmasyan, A., Batinic-Haberle, I., Vander Kooi, C. W., Chi, W., Latif, A. A., Panchatcharam, M., Prachayasittikul, V., Butterfield, D. A., Vore, M., Moscow, J., and St Clair, D. K. (2016) Novel role of 4-hydroxy-2-nonenal in AIFm2-mediated mitochondrial stress signaling. *Free Radic Biol Med* **91**, 68-80
49. Batinic-Haberle, I., Cuzzocrea, S., Reboucas, J. S., Ferrer-Sueta, G., Mazzon, E., Di Paola, R., Radi, R., Spasojevic, I., Benov, L., and Salvemini, D. (2009) Pure MnTBAP selectively scavenges peroxynitrite over superoxide: comparison of pure and commercial MnTBAP samples to MnTE-2-PyP in two models of oxidative stress injury, an SOD-specific Escherichia coli model and carrageenan-induced pleurisy. *Free Radic Biol Med* **46**, 192-201
50. Celic, T., Spanjol, J., Bobinac, M., Tovmasyan, A., Vukelic, I., Reboucas, J. S., Batinic-Haberle, I., and Bobinac, D. (2014) Mn porphyrin-based SOD mimic, MnTnHex-2-PyP(5+), and non-SOD mimic, MnTBAP(3-), suppressed rat spinal cord ischemia/reperfusion injury via NF-kappaB pathways. *Free Radic Res* **48**, 1426-1442
51. Gauter-Fleckenstein, B., Fleckenstein, K., Owzar, K., Jiang, C., Batinic-Haberle, I., and Vujaskovic, Z. (2008) Comparison of two Mn porphyrin-based mimics of superoxide dismutase in pulmonary radioprotection. *Free Radic Biol Med* **44**, 982-989
52. Gauter-Fleckenstein, B., Reboucas, J. S., Fleckenstein, K., Tovmasyan, A., Owzar, K., Jiang, C., Batinic-Haberle, I., and Vujaskovic, Z. (2014) Robust rat pulmonary radioprotection by a lipophilic Mn N-alkylpyridylporphyrin, MnTnHex-2-PyP(5+). *Redox Biol* **2**, 400-410
53. Mackensen, G. B., Patel, M., Sheng, H., Calvi, C. L., Batinic-Haberle, I., Day, B. J., Liang, L. P., Fridovich, I., Crapo, J. D., Pearlstein, R. D., and Warner, D.

S. (2001) Neuroprotection from delayed postischemic administration of a metalloporphyrin catalytic antioxidant. *J Neurosci* **21**, 4582-4592

54. Miriyala, S., Spasojevic, I., Tovmasyan, A., Salvemini, D., Vujaskovic, Z., St Clair, D., and Batinic-Haberle, I. (2011) Manganese superoxide dismutase, MnSOD and its mimics. *Biochim Biophys Acta*
55. Saba, H., Batinic-Haberle, I., Munusamy, S., Mitchell, T., Lichti, C., Megyesi, J., and MacMillan-Crow, L. A. (2007) Manganese porphyrin reduces renal injury and mitochondrial damage during ischemia/reperfusion. *Free Radic Biol Med* **42**, 1571-1578
56. Weitzel, D. H., Tovmasyan, A., Ashcraft, K. A., Rajic, Z., Weitner, T., Liu, C., Li, W., Buckley, A. F., Prasad, M. R., Young, K. H., Rodriguiz, R. M., Wetsel, W. C., Peters, K. B., Spasojevic, I., Herndon, J. E., 2nd, Batinic-Haberle, I., and Dewhirst, M. W. (2015) Radioprotection of the brain white matter by Mn(III) n-Butoxyethylpyridylporphyrin-based superoxide dismutase mimic MnTnBuOE-2-PyP5+. *Mol Cancer Ther* **14**, 70-79
57. Spasojevic, I., Chen, Y., Noel, T. J., Fan, P., Zhang, L., Reboucas, J. S., St Clair, D. K., and Batinic-Haberle, I. (2008) Pharmacokinetics of the potent redox-modulating manganese porphyrin, MnTE-2-PyP(5+), in plasma and major organs of B6C3F1 mice. *Free Radic Biol Med* **45**, 943-949
58. Spasojevic, I., Chen, Y., Noel, T. J., Yu, Y., Cole, M. P., Zhang, L., Zhao, Y., St Clair, D. K., and Batinic-Haberle, I. (2007) Mn porphyrin-based superoxide dismutase (SOD) mimic, MnIIITE-2-PyP5+, targets mouse heart mitochondria. *Free Radic Biol Med* **42**, 1193-1200
59. Tovmasyan, A., Bueno-Janice, J. C., Jaramillo, M. C., Sampaio, R. S., Reboucas, J. S., Kyui, N., Benov, L., Deng, B., Huang, T. T., Tome, M. E., Spasojevic, I., and Batinic-Haberle, I. (2018) Radiation-Mediated Tumor Growth Inhibition Is Significantly Enhanced with Redox-Active Compounds That Cycle with Ascorbate. *Antioxid Redox Signal*
60. Carlioz, A., and Touati, D. (1986) Isolation of superoxide dismutase mutants in Escherichia coli: is superoxide dismutase necessary for aerobic life? *Embo J* **5**, 623-630
61. Munroe, W., Kingsley, C., Durazo, A., Gralla, E. B., Imlay, J. A., Srinivasan, C., and Valentine, J. S. (2007) Only one of a wide assortment of manganese-containing SOD mimicking compounds rescues the slow aerobic growth phenotypes of both Escherichia coli and Saccharomyces cerevisiae strains lacking superoxide dismutase enzymes. *J Inorg Biochem* **101**, 1875-1882
62. Okado-Matsumoto, A., Batinic-Haberle, I., and Fridovich, I. (2004) Complementation of SOD-deficient Escherichia coli by manganese porphyrin mimics of superoxide dismutase activity. *Free Radic Biol Med* **37**, 401-410
63. Tovmasyan, A., Reboucas, J. S., and Benov, L. (2013) Simple biological systems for assessing the activity of superoxide dismutase mimics. *Antioxid Redox Signal* **20**, 2416-2436
64. Tovmasyan, A. G., Rajic, Z., Spasojevic, I., Reboucas, J. S., Chen, X., Salvemini, D., Sheng, H., Warner, D. S., Benov, L., and Batinic-Haberle, I. (2011) Methoxy-derivatization of alkyl chains increases the in vivo efficacy of cationic Mn porphyrins. Synthesis, characterization, SOD-like activity, and SOD-deficient E. coli study of meta Mn(III) N-methoxyalkylpyridylporphyrins. *Dalton Trans* **40**, 4111-4121
65. Alvarez-Paggi, D., Hannibal, L., Castro, M. A., Oviedo-Rouco, S., Demicheli, V., Tortora, V., Tomasina, F., Radi, R., and Murgida, D. H. (2017)

Multifunctional Cytochrome c: Learning New Tricks from an Old Dog. *Chem Rev* **117**, 13382-13460

66. Capdevila, D. A., Oviedo Rouco, S., Tomasina, F., Tortora, V., Demicheli, V., Radi, R., and Murgida, D. H. (2015) Active Site Structure and Peroxidase Activity of Oxidatively Modified Cytochrome c Species in Complexes with Cardiolipin. *Biochemistry* **54**, 7491-7504
67. Ohta, T., Liu, J., and Naruta, Y. (2013) Resonance Raman characterization of mononuclear heme-peroxo intermediate models. *Coord Chem Rev* **257**, 407-413
68. Spiro, T. G., Soldatova, A. V., and Balakrishnan, G. (2013) CO, NO and O2 as Vibrational Probes of Heme Protein Interactions. *Coord Chem Rev* **257**, 511-527
69. Arellano, L. M., Barrejon, M., Gobeze, H. B., Gomez-Escalonilla, M. J., Fierro, J. L. G., D'Souza, F., and Langa, F. (2017) Charge stabilizing tris(triphenylamine)-zinc porphyrin-carbon nanotube hybrids: synthesis, characterization and excited state charge transfer studies. *Nanoscale* **9**, 7551-7558
70. Fernandez, C. C., Spedalieri, C., Murgida, D. H., and Williams, F. J. (2017) Surface Influence on the Metalation of Porphyrins at the Solid–Liquid Interface. *J Phys Chem C* **121**, 21324-21332
71. Romelt, C., Ye, S., Bill, E., Weyhermuller, T., van Gastel, M., and Neese, F. (2018) Electronic Structure and Spin Multiplicity of Iron Tetraphenylporphyrins in Their Reduced States as Determined by a Combination of Resonance Raman Spectroscopy and Quantum Chemistry. *Inorg Chem* **57**, 2141-2148
72. Schick, G. A., and Bocian, D. F. (1987) Resonance Raman studies of hydroporphyrins and chlorophylls. *Biochim Biophys Acta* **895**, 127-154
73. Batinic-Haberle, I., Spasojevic, I., Tse, H. M., Tovmasyan, A., Rajic, Z., St Clair, D. K., Vujaskovic, Z., Dewhirst, M. W., and Piganelli, J. D. (2012) Design of Mn porphyrins for treating oxidative stress injuries and their redox-based regulation of cellular transcriptional activities. *Amino Acids* **42**, 95-113
74. Rios, N., Piacenza, L., Trujillo, M., Martinez, A., Demicheli, V., Prolo, C., Alvarez, M. N., Lopez, G. V., and Radi, R. (2016) Sensitive detection and estimation of cell-derived peroxynitrite fluxes using fluorescein-boronate. *Free Radic Biol Med* **101**, 284-295
75. Radi, R., Beckman, J. S., Bush, K. M., and Freeman, B. A. (1991) Peroxynitrite oxidation of sulfhydryls. The cytotoxic potential of superoxide and nitric oxide. *J Biol Chem* **266**, 4244-4250
76. Saha, A., Goldstein, S., Cabelli, D., and Czapski, G. (1998) Determination of optimal conditions for synthesis of peroxynitrite by mixing acidified hydrogen peroxide with nitrite. *Free Radic Biol Med* **24**, 653-659
77. Hughes, M. N., Nicklin, H.G. (1968) The chemistry of pernitrites. Part I. Kinetics of decomposition of pernitrous acid. *J. Chem. Soc.* **A**, 450-456
78. Quijano, C., Castro, L., Peluffo, G., Valez, V., and Radi, R. (2007) Enhanced mitochondrial superoxide in hyperglycemic endothelial cells: direct measurements and formation of hydrogen peroxide and peroxynitrite. *Am J Physiol Heart Circ Physiol* **293**, H3404-3414
79. Royall, J. A., and Ischiropoulos, H. (1993) Evaluation of 2',7'-dichlorofluorescin and dihydrorhodamine 123 as fluorescent probes for intracellular H2O2 in cultured endothelial cells. *Arch Biochem Biophys* **302**, 348-355
80. Feelisch, M., Ostrowski, J., and Noack, E. (1989) On the mechanism of NO release from sydnonimines. *J Cardiovasc Pharmacol* **14 Suppl 11**, S13-22

81. Swintek, A. U., Christoph, S., Petrat, F., de Groot, H., and Kirsch, M. (2004) Cell type-dependent release of nitric oxide and/or reactive nitrogenoxide species from intracellular SIN-1: effects on cellular NAD(P)H. *Biol Chem* **385**, 639-648
82. Fiuza, B., Subelzu, N., Calcerrada, P., Straliotto, M. R., Piacenza, L., Cassina, A., Rocha, J. B., Radi, R., de Bem, A. F., and Peluffo, G. (2015) Impact of SIN-1-derived peroxynitrite flux on endothelial cell redox homeostasis and bioenergetics: protective role of diphenyl diselenide via induction of peroxiredoxins. *Free Radic Res* **49**, 122-132
83. Cassina, A., and Radi, R. (1996) Differential inhibitory action of nitric oxide and peroxynitrite on mitochondrial electron transport. *Arch Biochem Biophys* **328**, 309-316
84. Dranka, B. P., Hill, B. G., and Darley-Usmar, V. M. (2010) Mitochondrial reserve capacity in endothelial cells: The impact of nitric oxide and reactive oxygen species. *Free Radic Biol Med* **48**, 905-914
85. Ferrick, D. A., Neilson, A., and Beeson, C. (2008) Advances in measuring cellular bioenergetics using extracellular flux. *Drug Discov Today* **13**, 268-274
86. Gerencser, A. A., Neilson, A., Choi, S. W., Edman, U., Yadava, N., Oh, R. J., Ferrick, D. A., Nicholls, D. G., and Brand, M. D. (2009) Quantitative microplate-based respirometry with correction for oxygen diffusion. *Anal Chem* **81**, 6868-6878
87. Reers, M., Smith, T. W., and Chen, L. B. (1991) J-aggregate formation of a carbocyanine as a quantitative fluorescent indicator of membrane potential. *Biochemistry* **30**, 4480-4486
88. Blom, N., Odo, J., Nakamoto, K., and Strommen, D. P. (1986) Resonance Raman studies of metal tetrakis(4-N-methylpyridyl)porphine: band assignments, structure-sensitive bands, and species equilibria. *The Journal of Physical Chemistry* **90**, 2847-2852
89. Burke, J. M., Kincaid, J. R., Peters, S., Gagne, R. R., Collman, J. P., and Spiro, T. G. (1978) Structure-sensitive resonance Raman bands of tetraphenyl and "picket fence" porphyrin-iron complexes, including an oxyhemoglobin analog. *J. Am. Chem. Soc.* **100**, 6083-6088
90. Spiro, T. G. (1978) Resonance Raman spectra of hemoproteins. *Methods Enzymol* **54**, 233-249
91. Spiro, T. G., and Burke, J. M. (1976) Protein control of porphyrin conformation. Comparison of resonance Raman spectra of heme proteins with mesoporphyrin IX analogues. *J Am Chem Soc* **98**, 5482-5489
92. Odo, J., Mifune, M., Iwado, A., Karasudani, T., Hasimoto, H., Motohashi, N., Tanaka, Y., and Saito, Y. (1991) Resonance Raman Spectra of Manganese-Porphyrins on Ion-Exchange Resins Exhibiting Uricase-Like Catalytic Activity. *Anal Sci* **7**,
93. Spasojevic, I., Batinic-Haberle, I., and Fridovich, I. (2000) Nitrosylation of manganese(II) tetrakis(N-ethylpyridinium-2-yl)porphyrin: a simple and sensitive spectrophotometric assay for nitric oxide. *Nitric Oxide* **4**, 526-533
94. Koppenol, W. H., Moreno, J. J., Pryor, W. A., Ischiropoulos, H., and Beckman, J. S. (1992) Peroxynitrite, a cloaked oxidant formed by nitric oxide and superoxide. *Chem Res Toxicol* **5**, 834-842
95. Brown, G. C. (2001) Regulation of mitochondrial respiration by nitric oxide inhibition of cytochrome c oxidase. *Biochim Biophys Acta* **1504**, 46-57
96. Turrens, J. F. (2003) Mitochondrial formation of reactive oxygen species. *J Physiol* **552**, 335-344

97. Brito, P. M., Mariano, A., Almeida, L. M., and Dinis, T. C. (2006) Resveratrol affords protection against peroxynitrite-mediated endothelial cell death: A role for intracellular glutathione. *Chem Biol Interact* **164**, 157-166
98. Zhang, X., Chen, J., Graham, S. H., Du, L., Kochanek, P. M., Draviam, R., Guo, F., Nathaniel, P. D., Szabo, C., Watkins, S. C., and Clark, R. S. (2002) Intranuclear localization of apoptosis-inducing factor (AIF) and large scale DNA fragmentation after traumatic brain injury in rats and in neuronal cultures exposed to peroxynitrite. *J Neurochem* **82**, 181-191
99. de Bem, A. F., Fiuza, B., Calcerrada, P., Brito, P. M., Peluffo, G., Dinis, T. C., Trujillo, M., Rocha, J. B., Radi, R., and Almeida, L. M. (2013) Protective effect of diphenyl diselenide against peroxynitrite-mediated endothelial cell death: a comparison with ebselen. *Nitric Oxide* **31**, 20-30
100. Ferrer-Sueta, G., and Radi, R. (2009) Chemical biology of peroxynitrite: kinetics, diffusion, and radicals. *ACS Chem Biol* **4**, 161-177
101. Valez, V., Cassina, A., Batinic-Haberle, I., Kalyanaraman, B., Ferrer-Sueta, G., and Radi, R. (2013) Peroxynitrite formation in nitric oxide-exposed submitochondrial particles: detection, oxidative damage and catalytic removal by Mn-porphyrins. *Arch Biochem Biophys* **529**, 45-54

FIGURE LEGENDS

Figure 1. RR spectra of MnP. (A) High-frequency region RR spectra of MnTnBuOE-2-PyP^{5+} (50 μM) (top) and MnTnHex-2-PyP^{5+} (50 μM) (bottom) in PBS. The black and red lines represent the spectra of oxidized Mn(III)P and sodium dithionite-reduced Mn(II)P, respectively. **(B)** RR spectra of MnTnBuOE-2-PyP^{5+} (100 μM) in the presence of increasing concentrations of SIN-1 (100, 480 μM and 5 mM) (top), and MnTnBuOE-2-PyP^{5+} (100 μM) incubated with ascorbic acid (2 mM) and then added SIN-1 was added (150 μM and 2 mM) (bottom). Measurements were performed at 457.9 nm excitation, 5 mW laser power at sample and accumulation times of 40s (4 × 10s). Band assignment adopted from (88,92).

Figure 2. RR spectra of MnTnHex-2-PyP^{5+} incubated with isolated mitochondria tested with succinate and respiratory inhibitors. Controls: **(a)** Isolated mitochondria (0.5 mg/mL) in PBS; **(b)** Mn(III)TnHex-2-PyP^{5+} (5 μM) incubated with succinate (6 mM), rotenone (1 μM) and malonate (10 mM), in the absence of mitochondria and **(c)** Mn(III)TnHex-2-PyP^{5+} added to mitochondria, in the absence of succinate. Study of the redox state of MnP: **(d)** Mn(III)TnHex-2-PyP^{5+} incubated with mitochondria, in the presence of succinate (6 mM) and **(e)** rotenone (1 μM) and malonate (10 mM); **(f)** Mn(III)TnHex-2-PyP^{5+} incubated with mitochondria, in the presence of antimycin A (2.5 μM) and succinate (6 mM). Measurements were performed at 457.9 nm excitation, 5 mW laser power at sample and accumulation times of 160 s (8 × 20s).

Figure 3. RR spectra of MnP incubated with isolated mitochondria exposed to SIN-1. (A) In the absence of respiratory inhibitors: (a) isolated mitochondria (0.5 mg/mL) in PBS; **(b)** plus Mn(III)TnBuOE-2-PyP^{5+} (5 μM); **(c)** incubated with succinate (6 mM); **(d)** exposed to SIN-1 (200 μM) after 10 min. (B) In the presence of respiratory inhibitors: (a) isolated mitochondria (0.5 mg/mL) in PBS; **(b)** plus Mn(III)TnHex-2-PyP^{5+} (5 μM); **(c)** incubated with succinate (3 mM); **(d)** plus rotenone (1 μM) and TTFA (10 μM) and exposed to SIN-1 (200 μM) after 10 min. Measurements were performed at 457.9 nm excitation, 5 mW laser power at sample and accumulation times of 160 s (8 × 20s).

Figure 4. RR spectra of MnP incubated with BAEC. Confluent BAEC were incubated with Mn(III)TnBuOE-2-PyP^{5+} (5 μM) for 2 h. After treatment, cells were extensively washed with PBS, repeating three cycles of cell centrifugation at 1000 g for 5 min, pellet was resuspended in PBS and RR spectra were acquired. (a) Control:

BAEC in PBS; and (b) preincubated with Mn(III)TnHex-2-PyP^{5+}. Measurements were performed at 457.9 nm excitation, 5 mW laser power at sample and accumulation times of 480 s (8 × 60s).

Figure 5. RR spectra of MnP added to BAEC in the presence of respiratory inhibitors and SIN-1. BAEC were incubated with Mn(III)TnHex-2-PyP^{5+} (5 μM) and RR spectra were immediately acquired. **(a)** BAEC in PBS; **(b)** plus Mn(III)TnHex-2-PyP^{5+} (5 μM); **(c)** with succinate (3 mM); **(d)** plus rotenone (1 μM) and TTFA (10 μM); **(e)** with SIN-1 (250 μM); **(f)** after 20 min SIN-1 exposure. Measurements were performed at 457.9 nm excitation, 5 mW laser power at sample and accumulation times of 480 s (8 × 60s).

Figure 6. Kinetics of Mn(III)TnBuOE-2-PyP^{5+} reaction with peroxynitrite. (A) Kinetic traces of Mn(III)TnBuOE-2-PyP^{5+} reaction with excess peroxynitrite concentrations under pseudo-first order conditions. Mn(III)TnBuOE-2-PyP^{5+} (0.5 μM) in sodium phosphate buffer (50 mM, with 0.1 mM DTPA), was mixed with different peroxynitrite concentrations (from right to left: 2.5, 5, 7.5, 10 and 12.5 μM) at pH 7.2 and 37 °C, and followed at 455 nm. A is the absorbance at time t, and A_0 and A_{INF} are the initial and final values, respectively. *Inset.* Logarithmic plot of stopped-flow kinetic traces up to 0.03 s. **(B)** The observed rate constants k_{obs} (s^{-1}) were determined from the fit of the decay of Mn(III)TnBuOE-2-PyP^{5+} at 455 nm to a single exponential function. Results are the mean ± standard deviation ($n \geq 7$) of a typical experiment. The second-order rate constant was determined from the slope of the plot of k_{obs} versus peroxynitrite concentrations. **(C)** pH-dependence of the reaction. The k_{obs} of Mn(III)TnBuOE-2-PyP^{5+} oxidation was determined at each peroxynitrite concentration and pH value. The

apparent second-order rate constants (k_{app}) obtained from the plot of k_{obs} versus peroxynitrite concentrations were plotted as a function of pH. Solid line represents the best fit to equation: $k_{app} = k_1K_a/(K_a + [H^+])$, where k_1 is the rate constant between $ONOO^-$ and the Mn(III)P and K_a represent a ionization constant of ONOOH.

Figure 7. Effect of MnP on cell-derived peroxynitrite generation in endothelial cells. Confluent BAEC monolayers were preincubated with Mn(III)TnBuOE-2-PyP^{5+} (5 μM) as described in experimental procedures section. Then, cells were incubated with Fl-B (50 μM, in PBS for 30 min) and stimulated intra-mitochondrial peroxynitrite generation by antimycin A (4 μM) treatment in the presence or in the absence of NOC-7 (100 μM), as indicated. The time course of the increase in the fluorescence intensity emission corresponding to Fl-B oxidation in the different cellular conditions were measured in a fluorescent microplate reader ($\lambda_{ex/em}$ = 492/515 nm). Slopes were calculated from the primary data set. For clarity, only selected time courses of fluorescence are shown (inset). Data are the means ± the standard error of the mean (SEM) of three independent experiments. *P < 0.03 indicates statistical difference when compared each condition with and without MnP by *t*-test unpaired with Welch´s correction. P < 0.0001 by one-way ANOVA test.

Figure 8. Measurement of mitochondrial function in BAEC. Cells were preincubated with Mn(III)TnBuOE-2-PyP^{5+} (5 μM) for 2 h, washed and exposed to SIN-1 (100 μM) as described in experimental procedures. **(A)** Representative time course for oxygen consumption rate measurements (QO_2). Sequential addition of oligomycin (1 μM), FCCP (1 μM) and antimycin A plus rotenone (AA/R:1 μM/0.1

μM). This progress curve shows basal respiratory rate **(B)** and after addition of oligomycin and FCCP, ATP-linked respiration **(C)**, spare respiratory capacity **(D)** and RCR **(E)**, were calculated as described above. Data represent the mean ± the standard error of the mean (SEM) of at least 4 group of independent experiments (n≥8 per group) and are expressed as oxygen consumption rates (pmol/min/μg protein). Asterisks indicate statistically significant differences (*P < 0.0007, **P < 0.007 and *** P < 0.03) by *t*-test unpaired with Welch´s correction. P < 0.006 by one-way ANOVA test.

Figure 9. Role of MnP in cellular mitochondrial membrane potential exposed to SIN-1. BAEC were preincubated with Mn(III)TnBuOE-2-PyP^{5+} (5 μM) for 2 hours and then treated with SIN-1 (100 μM) overnight. After that, cells were loaded with JC-1 (2 μM) and aggregate (590 nm, left column images) and monomer distribution (525 nm, center column images) were observed. Contrast and brightness of the top images were enhanced using Image J; exactly the same parameters were used in both images.

Figure 10. Evaluation of apoptosis triggered by SIN-1 and protection by MnP. BAEC were pretreated with Mn(III)TnBuOE-2-PyP^{5+} (5 μM) for 2 h, washed twice and then exposed to SIN-1 (250 μM) overnight. (A) Cells were harvested, and phosphatidyl serine externalization was evaluated by Annexin-Alexa-488 staining. Results were analyzed by flow cytometry and apoptotic cell labeling is given in arbitrary units. Results were expressed as the percentage of Annexin V-positive control cells (non-treated cells, traced line) and represent the mean ± SEM of at least three independent experiments. Asterisks indicate statistically significant differences (*P < 0.05) when

compared with control (non-treated cells) by one-way ANOVA test. (B) Representative flow cytometer histogram of Annexin V staining.

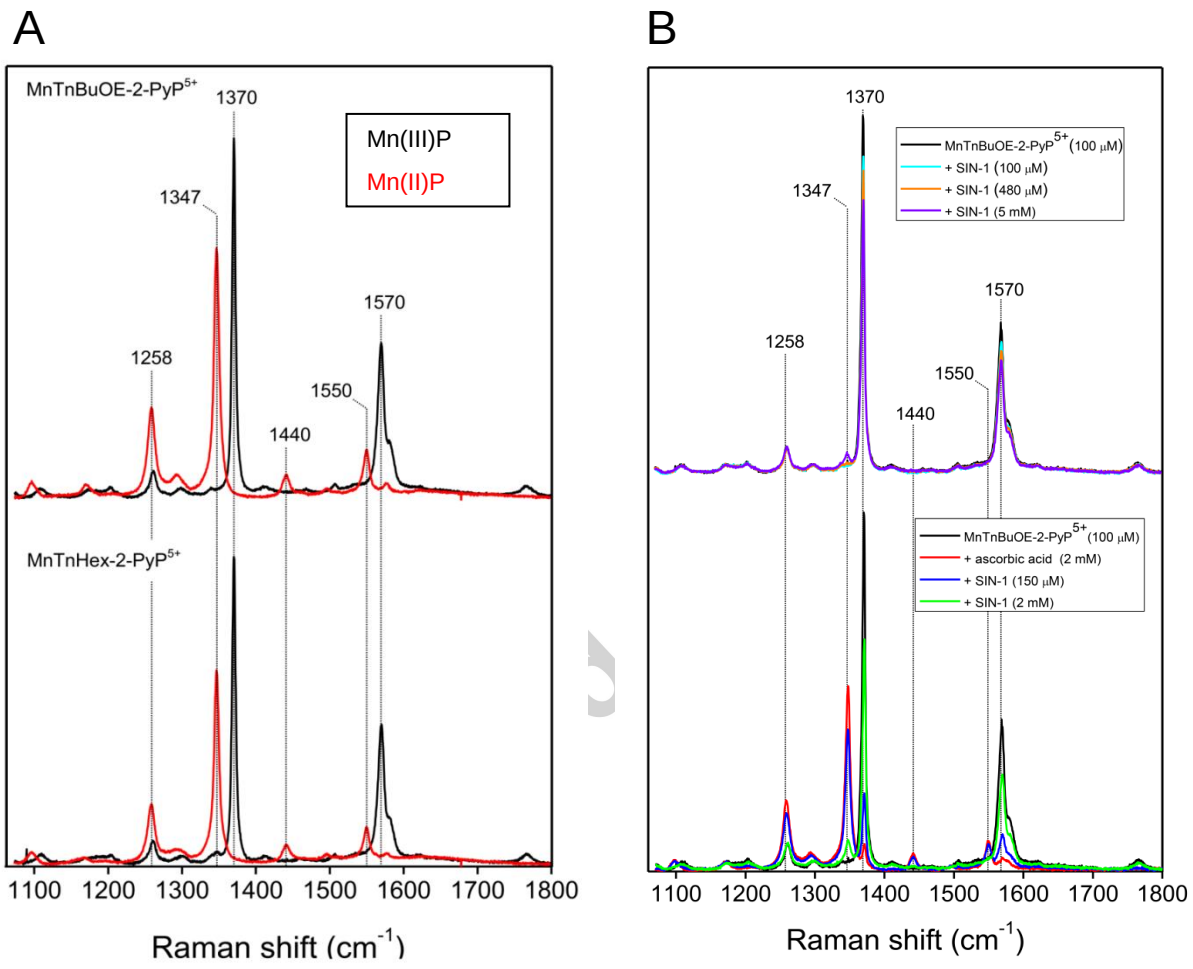

Figure 1

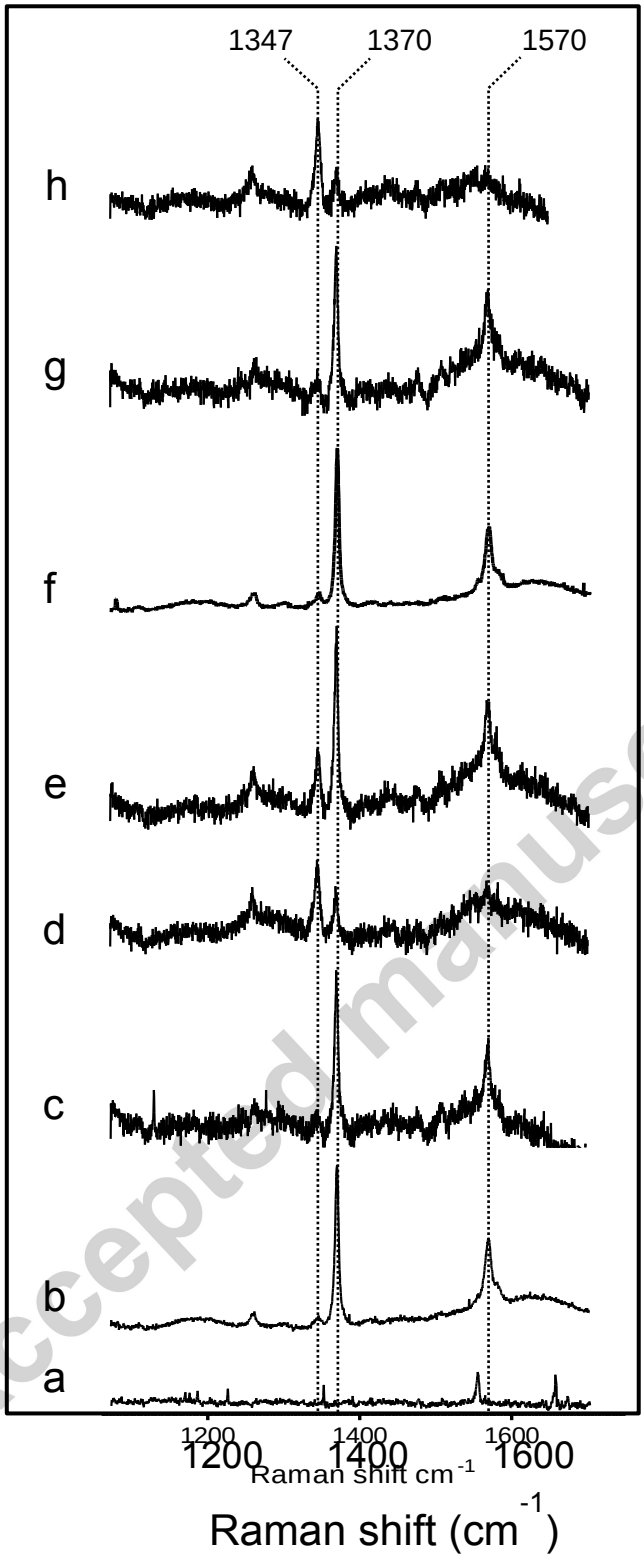

Figure 2

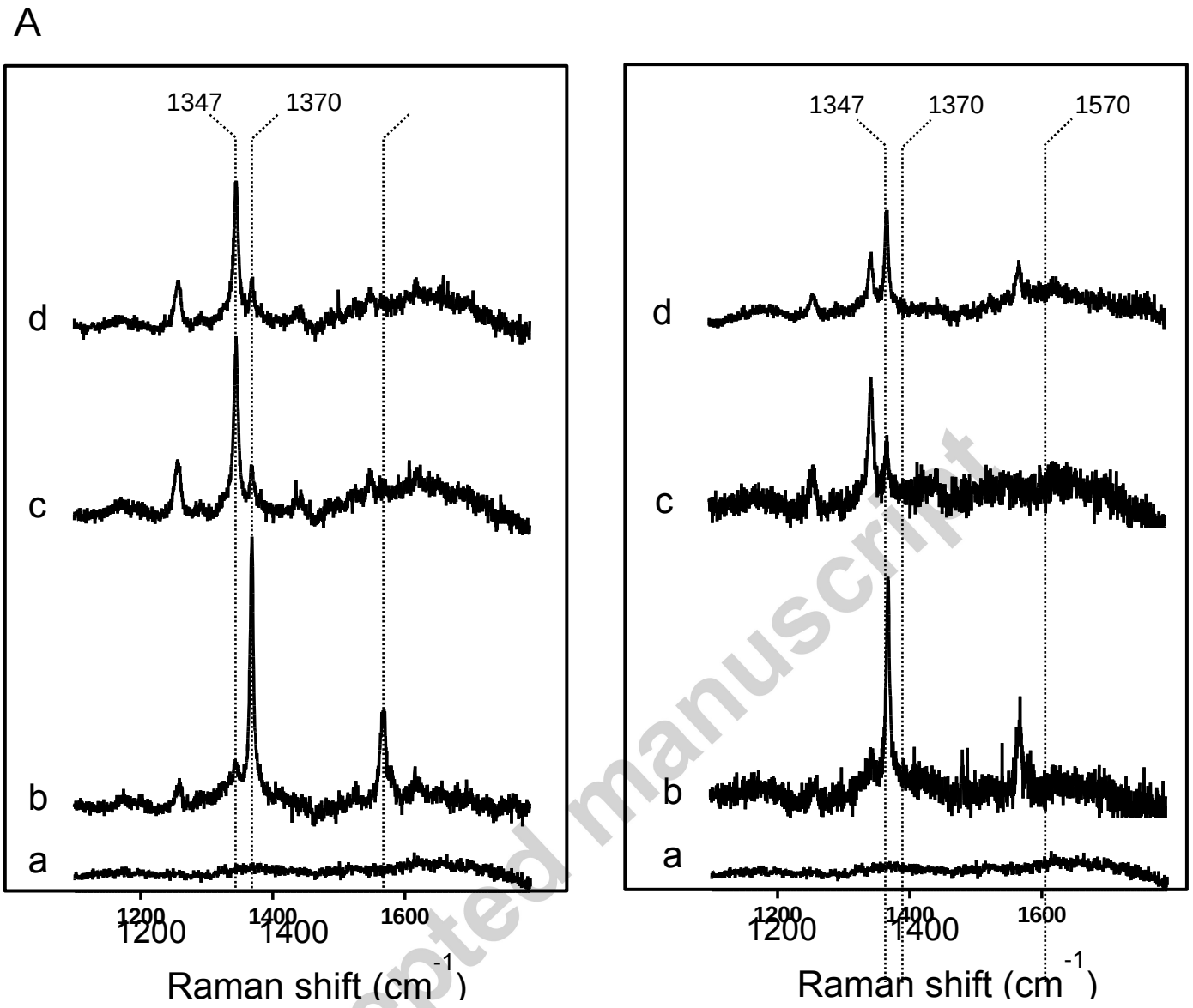

Figure 3

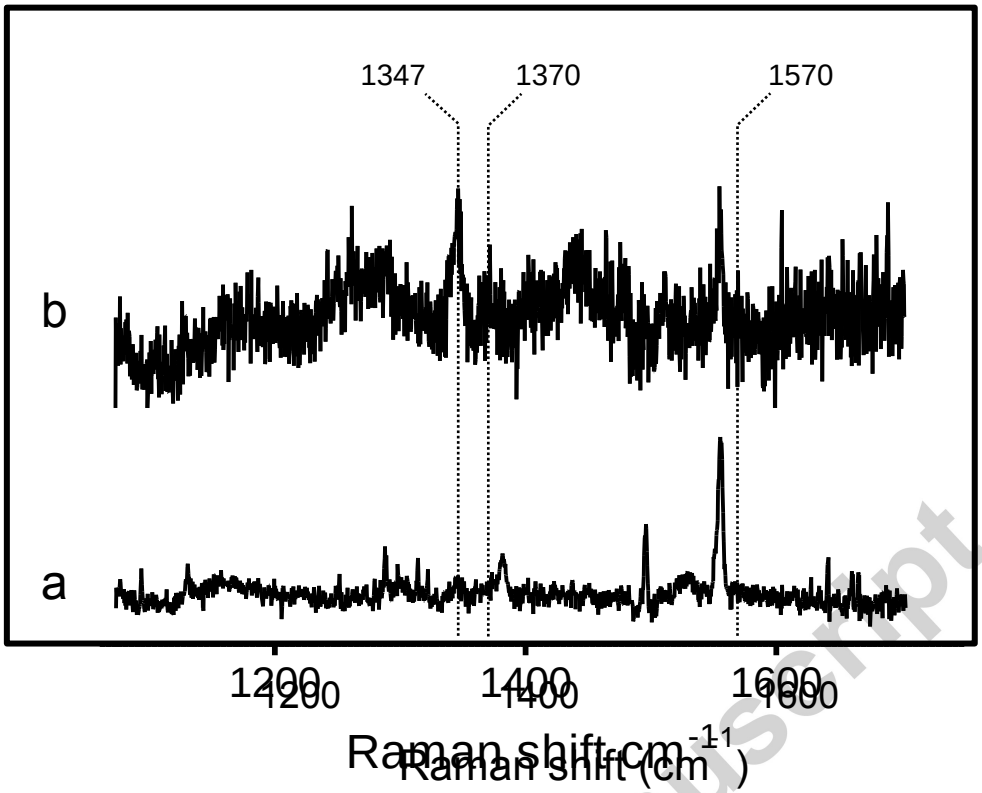

Figure 4

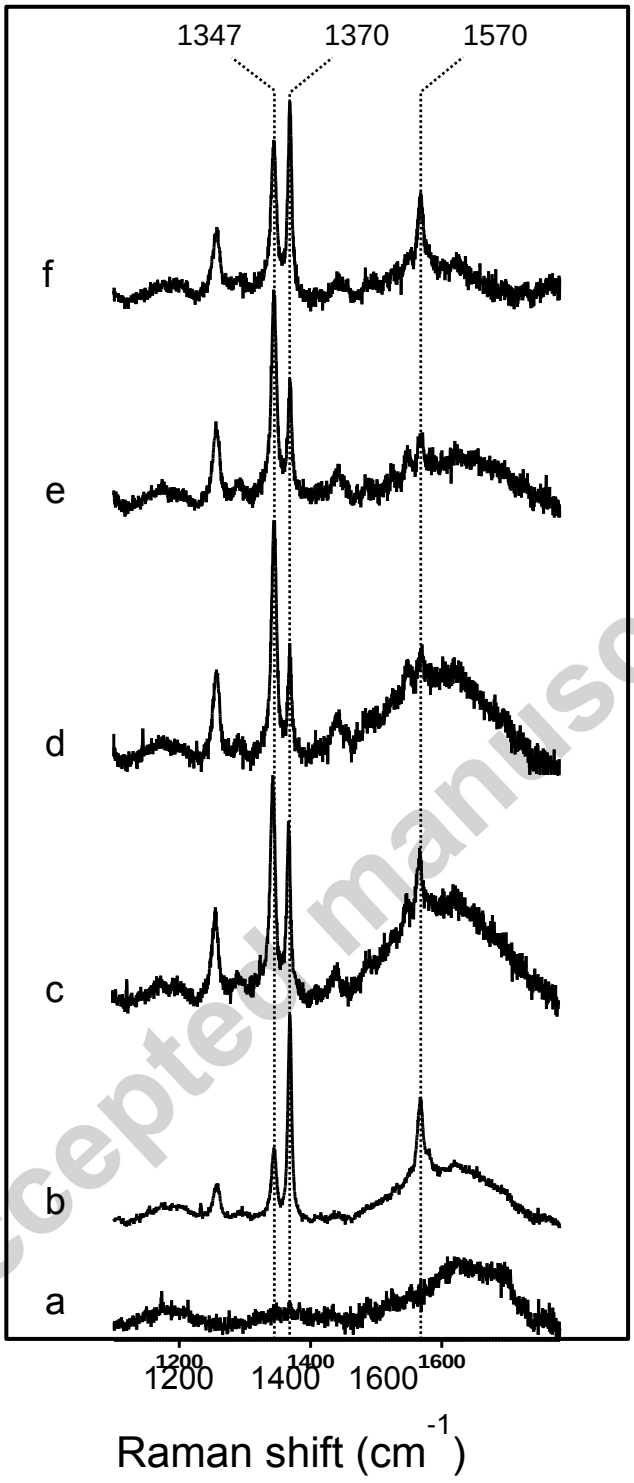

Figure 5

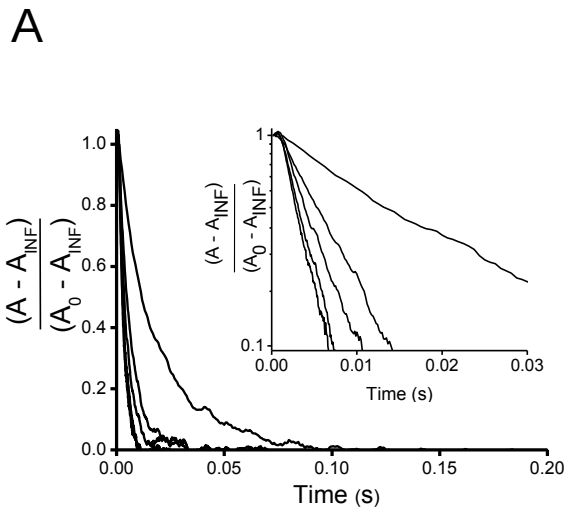

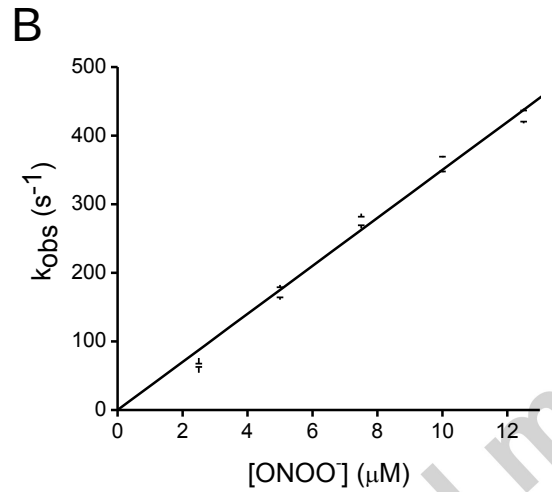

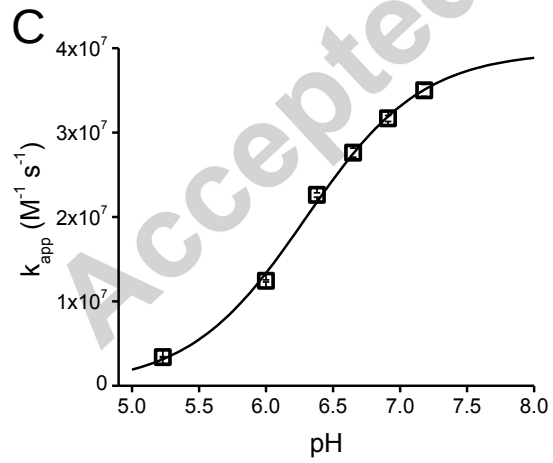

Figure 6

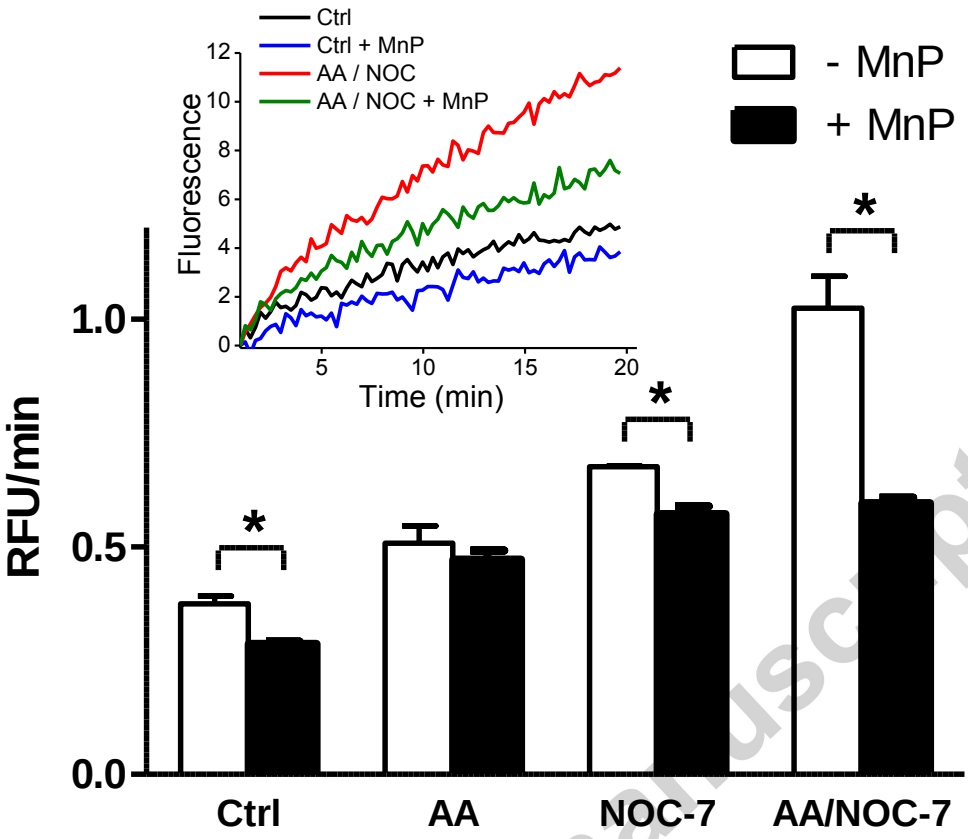

Figure 7

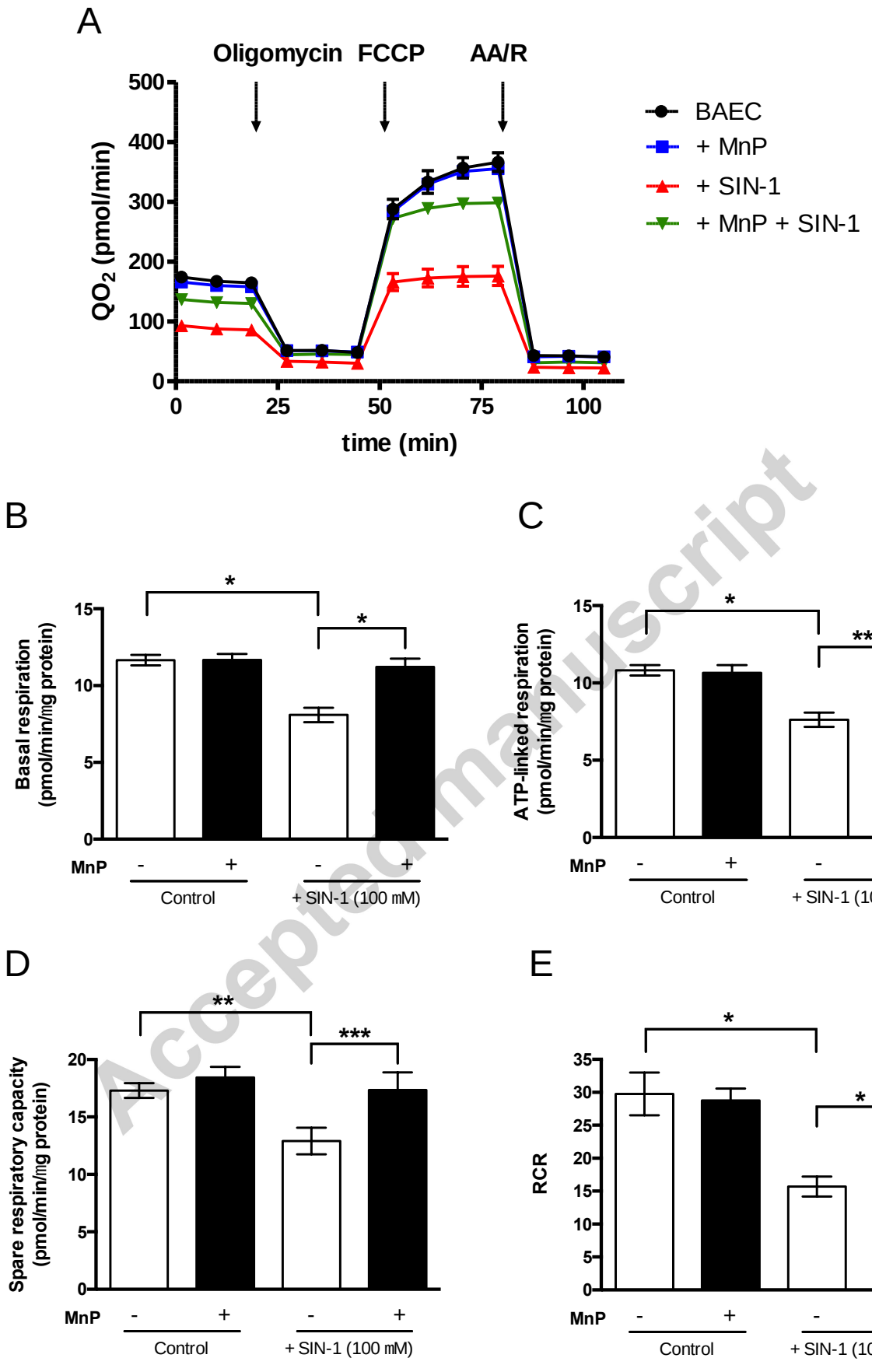

Figure 8

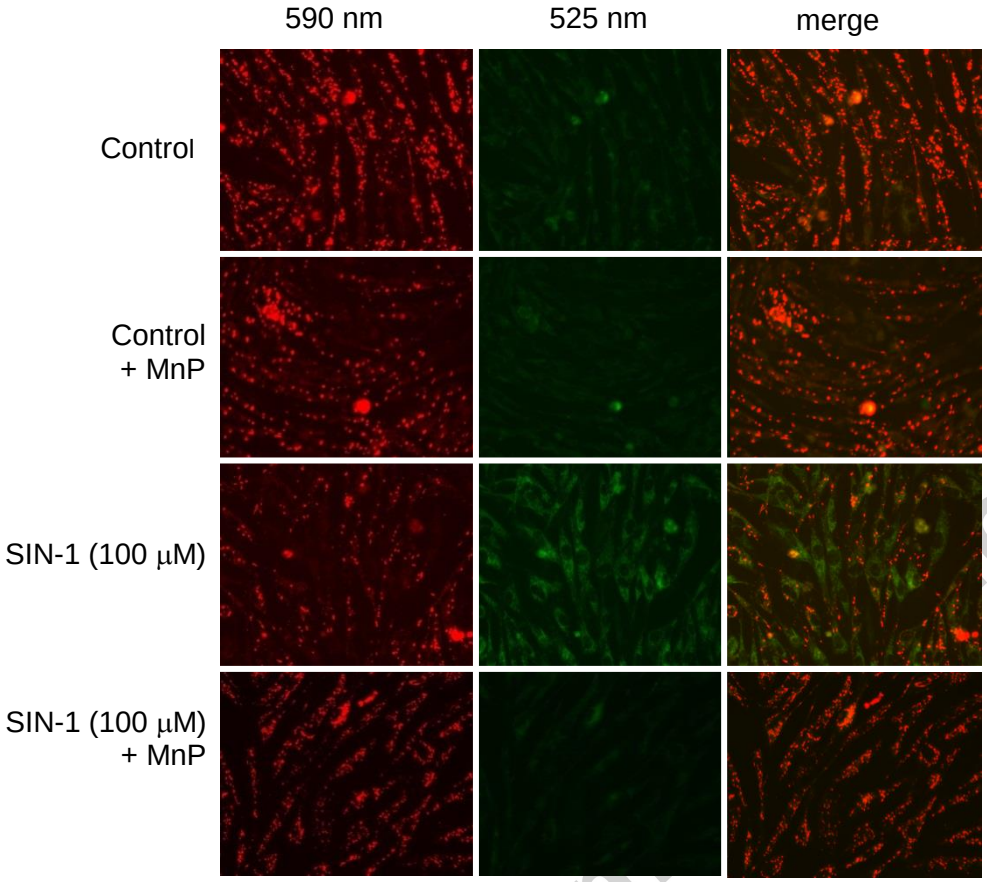

Figure 9

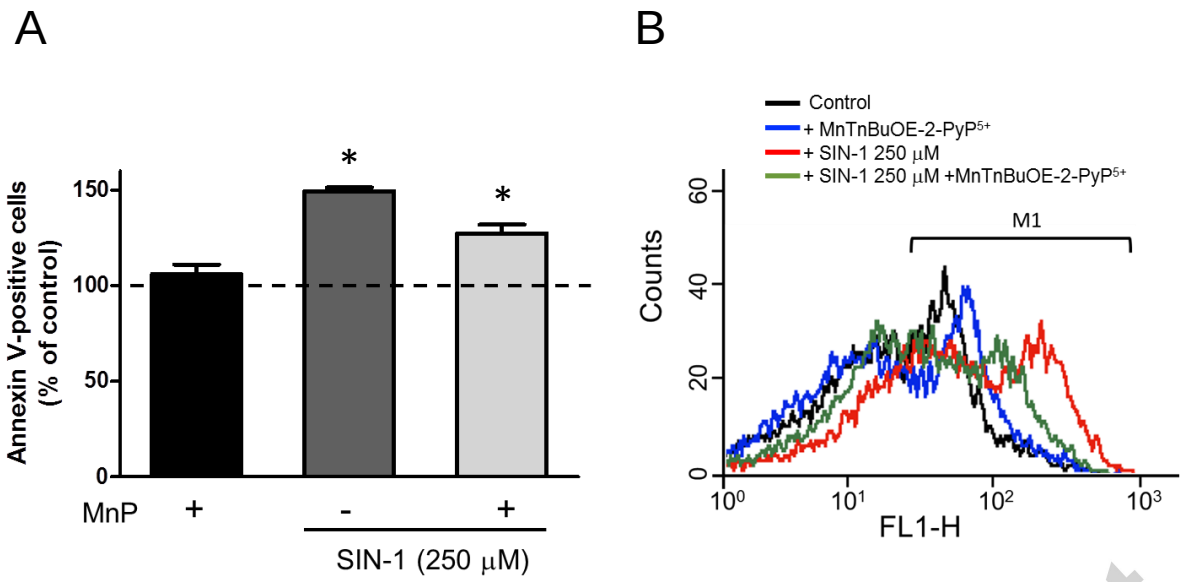

Figure 10

Highlights

- Raman Resonance was utilized to reveal the redox state of Mn-porphyrins (MnP) in cells
- Mn(III)P are readily reduced intracellularly to the Mn(II) state
- Intramitochondrial oxidation of a peroxynitrite-sensitive probe is inhibited by MnP
- The cytotoxicity of peroxynitrite is neutralized by MnP via a catalytic redox cycle